A&A 465, 559–573 (2007)
DOI: 10.1051/0004-6361:20066204

Astronomy & Astrophysics

Discovery of X-ray burst triplets in EXO 0748-676⋆

L. Boirin[1], L. Keek[2,3], M. Méndez[2,4], A. Cumming[5], J. J. M. In 't Zand[2,3], J. Cottam[6], F. Paerels[7], and W. H. G. Lewin[8]

[1] Observatoire Astronomique de Strasbourg, Université Louis Pasteur, 11 rue de l'Université, 67000 Strasbourg, France
e-mail: boirin@astro.u-strasbg.fr
[2] SRON, Netherlands Institute for Space Research, Sorbonnelaan 2, 3584 CA Utrecht, The Netherlands
[3] Astronomical Institute, Utrecht University, Princetonplein 5, 3584 CC Utrecht, The Netherlands
[4] Astronomical Institute "Anton Pannekoek", University of Amsterdam, Kruislaan 403, 1098 SJ Amsterdam, The Netherlands
[5] Physics Department, McGill University, 3600 Rue University, Montreal, QC H3A 2T8, Canada
[6] NASA Goddard Space Flight Center, Laboratory for X-ray Astrophysics, Greenbelt, Maryland 20771, USA
[7] Columbia Astrophysics Laboratory, 550 West 120th St., New York, NY 10027, USA
[8] Center for Space Research, Massachusetts Institute of Technology, 77 Massachusetts Avenue, Cambridge, MA 02139, USA

Received 7 August 2006 / Accepted 16 January 2007

ABSTRACT

Type-I X-ray bursts are thermonuclear flashes that take place on the surface of accreting neutron stars. The wait time between consecutive bursts is set by the time required to accumulate the fuel needed to trigger a new burst; this is at least one hour. Sometimes secondary bursts are observed, approximately 10 min after the main burst. These short wait-time bursts are not yet understood. We observed the low-mass X-ray binary and X-ray burster EXO 0748-676 with XMM-Newton for 158 h, during 7 uninterrupted observations lasting up to 30 h each. We detect 76 X-ray bursts. Most remarkably, 15 of these bursts occur in burst triplets, with wait times of 12 min between the three components of the triplet, T1, T2, and T3. We also detect 14 doublets with similar wait times between the two components of the doublet, D1 and D2. We characterize this behavior to try and obtain a better understanding of bursts with short wait times. We measure the burst peak flux, fluence, wait time and time profile, and study correlations between these parameters and with the persistent flux representing the mass accretion rate. (i) For all bursts with a long wait time, the fluence is tightly correlated with the wait time, whereas burst with short wait times generally have higher fluences than expected from this relationship; (ii) wait times tend to be longer after doublets and triplets; (iii) the time profile of single bursts, S1, and of the first burst in a double or triple burst, D1 and T1, always contains a slow component which is generally absent in the D2, T2 and T3 bursts; (iv) the peak flux is highest for S1, D1 and T1 bursts, but this is still a factor of 7 lower than the highest peak flux ever seen for a burst in this system; (v) the persistent flux, representing the mass accretion rate onto the neutron star, is about 1% of Eddington, which is among the lowest value so far measured for this system. The amount of energy per gram of accreted mass liberated during bursts is consistent with a fuel mixture of hydrogen-rich material. The characteristics of the bursts indicate that possibly all bursts in this system are hydrogen-ignited, in contrast with most other frequent X-ray bursters in which bursts are helium-ignited, but consistent with the low mass accretion rate in EXO 0748-676. Possibly the hydrogen ignition is the determining factor for the occurrence of short wait-time bursts. For example the 12 min wait time may be associated with a nuclear beta decay timescale.

Key words. X-rays: binaries – X-rays: bursts – X-rays: individuals: EXO 0748-676

1. Introduction

Type I X-ray bursts are due to unstable burning of hydrogen and/or helium on the surface on an accreting neutron star (for a review see Lewin et al. 1993). Fuel accumulates for hours to days, and then ignites as soon as the pressure and temperature conditions for thermonuclear reactions are reached. Since the nuclear reaction rates depend strongly on the temperature, the ignition leads to a runaway process, and the fuel burns explosively in a rapid ∼10−100 s burst releasing typically 10^{38-39} erg. Two bursts from a given source are usually separated by a few hours. However, doublets with burst intervals as short as ∼10 min have been observed from several sources including EXO 0748-676 (Gottwald et al. 1986), GS 0836–429 (Aoki et al. 1992), 4U 1608–522 (Murakami et al. 1980), 4U 1636−536 (Ohashi et al. 1982; Pedersen et al. 1982), 4U 1705–440 (Langmeier et al. 1987) and XB 1745–248 (Inoue et al. 1984). A burst interval as short as 50 s has been seen in MXB 1659-29 (Wijnands et al. 2002). Lewin et al. (1976) report SAS-3 observations of *three* consecutive bursts from MXB 1743-28 with burst intervals of 18 and 4 min. However, these are observations of a field with several known bursters, and therefore there is a slight chance that these three bursts may not be attributed to one source.

Bursts separated by short time intervals are not well understood in the context of the classical thermonuclear flash model. Since the interval is too short to accrete sufficient material to fuel a thermonuclear burst, secondary bursts are thought to be due to burning of residual fuel that did not burn during the primary burst. This involves incomplete nuclear burning, fuel storage and a mixing mechanism with the freshly accreted material (Fujimoto et al. 1987).

EXO 0748-676 is one of the sources where the double burst phenomenon was best studied thanks to several EXOSAT observations carried out at different persistent fluxes of the system. In 1985, 26 bursts were detected, including four doublets with a burst separation of the order of 10−20 min (Gottwald et al. 1986). The doublets only occurred when the persistent flux was

⋆ Appendix is only available in electronic form at http://www.aanda.org

Table 1. XMM-Newton observations of EXO 0748-676 performed between September 19 and November 12, 2003. We indicate the observation identification and revolution numbers, the EPIC PN start and exposure times, the number of X-ray bursts and bursting events observed (for singlets, doublets and triplets separately and in total), and the mean event wait time.

Obs-ID	Rev.	Start (UT)			t_{exp}	Bursts	Singlets	Doublets	Triplets	Events	Mean event wait time
		Month	Day	h:m	(h)						(h)
0160760101	692	Sep.	19	13:37	24.6	10	6	2	0	8	3.20
0160760201	693	Sep.	21	13:38	25.1	14	6	1	2	9	2.65
0160760301	694	Sep.	23	10:42	30.0	14	7	2	1	10	3.02
0160760401	695	Sep.	25	17:29	20.4	[a] 9	3	[a] 3	0	[a] 6	3.49
0160760601	708	Oct.	21	10:02	15.2	8	3	1	1	5	2.99
0160760801	710	Oct.	25	19:19	17.3	9	3	3	0	6	2.71
0160761301	719	Nov.	12	08:24	25.2	12	5	2	1	8	3.19
		Total			157.9	76	33	14	5	52	Mean 3.02

[a] Including a burst detected by RGS only, a few seconds before EPIC cameras were turned on.

low. As the persistent flux increased, the doublet phenomenon stopped, the wait time of the single bursts increased, and their shape changed from a "slow" (long tail) to a "fast" profile sometimes showing photospheric expansion. Gottwald et al. (1986) hypothesized that these variations could be caused by the flashes changing from hydrogen-triggered hydrogen-helium flashes at low accretion rates to helium-dominated flashes at high accretion rates, a scenario previously theoretically studied by Fujimoto et al. (1981, see also Ayasli & Joss 1982) who outlined three ways to trigger shell flashes depending on the accretion rate. Gottwald et al. (1986) speculated that double bursts could be a feature of hydrogen-triggered hydrogen-helium flashes.

In another EXOSAT observation in 1986, 11 bursts were observed and showed a regular pattern with a long recurrence time always followed by a short one, reminiscent of the double burst phenomenon, but with longer separations, in the range 20−70 min (Gottwald et al. 1987). The wait time to a burst and the total emitted energy in that burst displayed a linear relation but with an offset energy at zero burst interval that was interpreted as incomplete consumption of fuel in the primary burst and its subsequent consumption in the secondary burst. The amount of unburned fuel was estimated to be 10−15% of the total available nuclear energy.

Cottam et al. (2002) reported redshifted spectral lines identified with O and Fe transitions during X-ray bursts from EXO 0748-676 observed with RGS on XMM-Newton, implying a gravitational redshift $z = 0.35$. Combining this redshift measurement with the peak flux of the radius expansion burst observed by Wolff et al. (2005) and the flux and color temperature observed during the cooling tail of bursts from EXOSAT and RXTE, Özel (2006) derived limits on EXO 0748-676 compact object mass and radius which ruled out several soft equations of state for the neutron star interior.

Özel (2006) further derived a lower limit to the EXO 0748-676 distance of 9.2 ± 1.0 kpc (see note 1 in Sect. 6). The source distance was previously estimated from bursts showing photospheric expansion to range between 6.8 and 9.1 kpc (Jonker & Nelemans 2004) or between 5.9 ± 0.9 and 7.7 ± 0.9 kpc (Wolff et al. 2005), the smallest and largest values corresponding to hydrogen rich and poor material, respectively. In this paper, we use the extreme values of the distance derived so far: 5 and 10 kpc.

EXO 0748-676 light curves exhibit dipping activity and eclipses every 3.8 h (e.g. Parmar et al. 1986). Dips and eclipses are due to the central X-ray source being obscured by some structure above the disk, and occulted by the companion star, respectively, at every orbital period (e.g. Frank et al. 1987). Their presence indicates that EXO 0748-676 is viewed at an inclination of ≈75−83° (Parmar et al. 1986), i.e. almost from the accretion disk plane.

Here, we report the discovery of *triple* bursts in EXO 0748-676. This is the first time that unambiguously and repeatedly triple bursts are detected in an accreting neutron star. We inspect EXO 0748-676 non-bursting emission to conclude that the accretion rate is likely constant throughout the analyzed set of XMM-Newton observations (Sect. 3). We derive the properties of the 76 bursts detected, using the 5−10 keV light curve to minimize the contamination from the dipping activity (Sect. 4). We perform a time-resolved spectral analysis of a sample of bursts not affected by dipping. We compare the triple bursts with the single and double bursts detected during the same XMM-Newton observations, and also with those detected during the EXOSAT observations (Sect. 5). We discuss the burst properties in the context of the well-studied helium-triggered hydrogen-helium burning thermonuclear flash model and in the context of the poorly-studied hydrogen-triggered hydrogen(-helium?) burning flash model (Sect. 6).

2. Observations and data reduction

The XMM-Newton Observatory (Jansen et al. 2001) includes three 1500 cm^2 X-ray telescopes each with a European Photon Imaging Camera (EPIC) at the focus. Two of the EPIC imaging spectrometers use MOS CCDs (Turner et al. 2001) and one uses PN CCDs (Strüder et al. 2001). Reflection Grating Spectrometers (RGS, den Herder et al. 2001) are located behind two of the telescopes.

EXO 0748-676 was observed by XMM-Newton on several occasions with different instrument configurations. In this paper, we use the 7 observations performed between September and November 2003, during XMM-Newton revolutions 692 to 719, for a total exposure time of 158 h (Table 1). We focus on the EPIC PN data (0.1−10 keV) that were all obtained in small window mode with the medium optical blocking filter applied. In this mode, only a fraction of the central CCD chip, corresponding to 63×64 pixels or $4\farcm3 \times 4\farcm4$, is read out. This allows a time resolution of 5.7 ms to be reached, and significant photon pile-up occurs only for count rates $\gtrsim$100 counts s^{-1}.

We reduce the observations using versions 5.4.1 to 6.1.0 of the science analysis software. Only single and double events (patterns 0 to 4) are selected. The ratio of background to source persistent intensity is generally $\lesssim$1% and reaches occasionally ∼10% during some episodes of higher background level due to enhanced solar activity. We do not discard any data interval

for this analysis. For the light curves and estimate of rough burst properties (peak count rates, number of counts in a burst), we extract source events from within a circle of 40″ radius centered on the position of EXO 0748-676. For the burst spectral analysis, we extract source events from an annulus with an outer radius of 40″ and a 9.3″ inner radius, in order to avoid pile-up effects which become significant near the burst peaks. Such an annulus contains 63% of the events from the circular region.

3. Non-bursting emission

The PN light curves of the 7 observations of EXO 0748-676 are shown in Fig. A.1 in the appendix, in the "hard" 5–10 keV (panel a) and in the "soft" 0.3−5 keV energy band (panel b), while panel c shows the color (counts in the hard band divided by those in the soft band) as a function of time. In addition to X-ray bursts, EXO 0748-676 light curves exhibit eclipses every 3.8 h and dipping activity.

Dipping is associated with spectral hardening (Fig. A.1c), the soft light curve (Fig. A.1b) being substantially more affected than the hard one (Fig. A.1a). The dipping activity is highly irregular on timescales of days, with the soft light curve shape clearly changing from one XMM-Newton observation to another. While a dipping pattern covering a limited phase range of ∼0.7−0.9 is easily recognizable in some observations (e.g. revolution 693), this is not the case in others (e.g. revolution 692) where the soft intensity and hardness display erratic variability at all orbital phases.

Díaz Trigo et al. (2006) analyzed the PN data of EXO 0748-676 during revolution 719. Excluding eclipses and bursts, they define six intensity stages, and call the highest range the "persistent" level, and the lowest one the "Dip 5" level. They extract one spectrum per level and fit them simultaneously with a continuum model affected by a neutral and by an ionized absorber. While the parameters of the continuum are forced to be the same for the six spectra, the parameters of the absorbers are left independent. By successfully fitting the spectra with this method, Díaz Trigo et al. (2006) demonstrate that all the intensity and spectral changes from EXO 0748-676 during revolution 719 can be simply explained by changes in the ionization level and in the amount of the absorbers that are located inside the system, while the underlying X-ray source is staying constant. Not only the "dipping" spectra are affected by the local absorbers, but also the "persistent" one (see Fig. 3 and Table 7 of Díaz Trigo et al. 2006). The term "persistent", if understood as un-affected by local absorbers, is therefore un-appropriate in this case, EXO 0748-676 being "dipping" (if understood as affected by local absorbers) at all intensity levels and at all phases during that observation.

In Fig. 1, we show the color-intensity diagram of the non-bursting emission of EXO 0748-676 during all the XMM-Newton revolutions examined here (from 692 to 719). Remarkably, the data from the different observations overlap perfectly in this diagram. Since the intensity and spectral changes during revolution 719, and hence the boomerang-like track associated with that revolution in Fig. 1, could be explained by changing absorbers in front of a constant X-ray source, we deduce that the spectral changes during the other observations, and thus their associated boomerang tracks in Fig. 1, can be explained similarly and that the underlying X-ray emission is the same during revolutions 692 to 719. If the underlying X-ray emission had been different from one observation to another, the various tracks would have appeared shifted with respect to each other, rather than being overlapping, unless a change in the underlying X-ray emission had the very same spectral signature in the color-intensity diagram as the change due to the absorbers, which is unlikely.

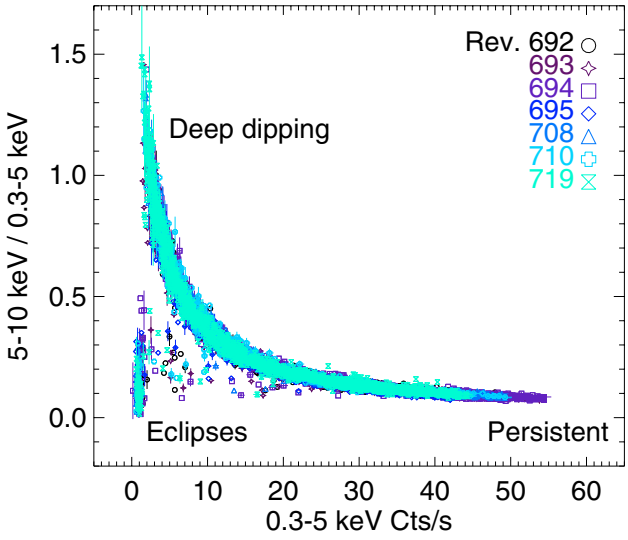

Fig. 1. Color (counts in the 5–10 keV band divided by counts in the 0.3−5 keV band) of EXO 0748-676 non-bursting emission as a function of the soft (0.3−5 keV) intensity during the 7 XMM-Newton observations whose revolution number is indicated in the right corner. Error bars are shown on one third of the points which represent 60 s each. The intensity and spectral changes during revolution 719 (bursts and eclipses excluded), and hence the boomerang track associated to that revolution, can be explained by changes in the ionization level and in the amount of absorbers in front of a constant underlying X-ray source (Díaz Trigo et al. 2006). Remarkably, the data obtained during the other revolutions (spanning several months) follow the same track. This indicates that the spectral changes during these observations can be explained by the same phenomenon and that the underlying X-ray emission is likely the same during the 7 observations studied here.

Therefore, in this paper, we assume a constant underlying X-ray flux, and hence a constant accretion rate, for EXO 0748-676 throughout the observations 692 to 719. We will consider the unabsorbed X-ray flux derived by Díaz Trigo et al. (2006) from revolution 719 as representative of the unabsorbed flux for all the observations studied here. We note that the maximum PN count rate reached by EXO 0748-676 outside bursts varies at most by a factor 1.3 from one observation to another, which could be considered an upper limit to the variation of the underlying flux, if the above-mentioned interpretation of changing absorbers in front of a constant underlying X-ray emitter throughout revolutions 692 to 719 was not correct.

Using the data from revolution 719, Díaz Trigo et al. (2006) derive a persistent 0.6−10 keV absorbed flux of 2.25×10^{-10} erg cm^{-2} s^{-1}. This corresponds to a 0.6−10 keV unabsorbed (without any attenuation) flux of 2.81×10^{-10} erg cm^{-2} s^{-1}. Introducing a break at 50 keV (as found in the 0.1−100 keV BeppoSAX spectrum, Sidoli et al. 2005) in the power-law component of their model, we derive, in the 0.1−100 keV energy band, an unabsorbed flux of 8.44×10^{-10} erg cm^{-2} s^{-1} that we consider as the representative bolometric underlying flux of EXO 0748-676 for revolutions 692 to 719. At 5 kpc, this implies an unabsorbed luminosity of 8.44×10^{35} erg s^{-1} in the 0.6−10 keV band, and 2.52×10^{36} erg s^{-1} in the 0.1−100 keV band. At 10 kpc, this implies a luminosity of 3.36×10^{36} erg s^{-1} in the 0.6−10 keV band and 1.01×10^{37} erg s^{-1} in the 0.1−100 keV band. We

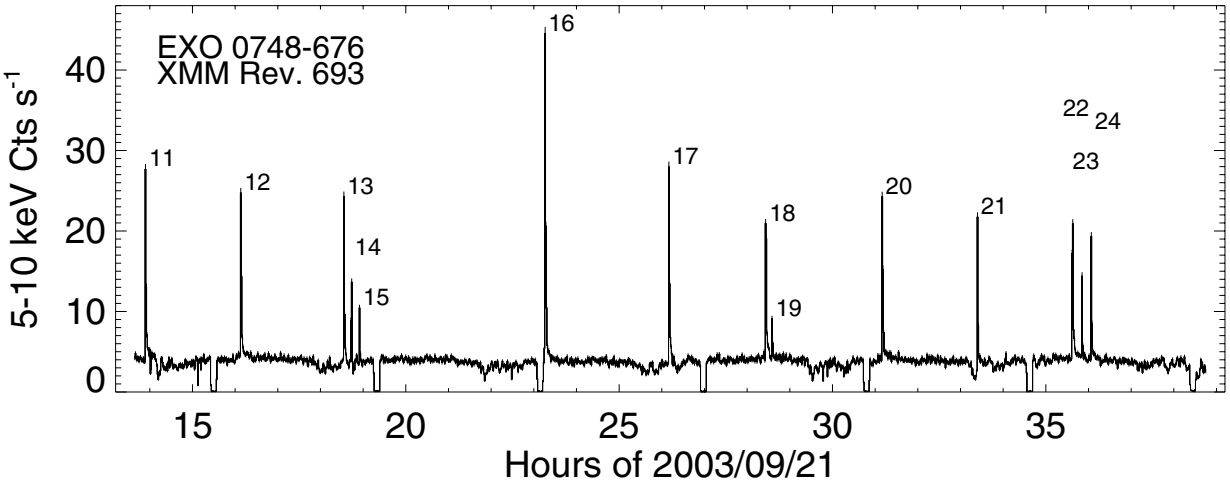

Fig. 2. 5–10 keV EPIC PN light curve of EXO 0748-676 with a binning of 60 s during XMM-Newton revolution 693. The X-ray bursts are numbered and occur either in singlets, doublets or triplets.

estimate the relative error on the fluxes and luminosities due to the spectral fit uncertainties to be ∼3%.

4. Bursts

76 X-ray bursts are recorded during the 7 XMM-Newton observations of EXO 0748-676 (Table 1). As illustrated in Figs. 2 and 3 (see also the complete set of bursts in Fig. A.1 of the appendix), most bursts occur after a wait time since a previous burst of typically 3 h, while others occur after a wait time of only ∼12 min. We will see in Sect. 4.2 that there is a clear distinction between these long and short wait-time bursts. We call several consecutive bursts separated by short wait times a *bursting event*. The observations contain events of one, two and three bursts, which we refer to as *singlets*, *doublets* and *triplets*, respectively. The burst types are denoted by S1 for a singlet, D1 and D2 for the first and second burst in a doublet, respectively, and T1, T2 and T3 for the first, second and third burst in a triplet, respectively.

The observations contain 52 bursting events: 33 singlets, 14 doublets and 5 triplets. On average, one event occurs every 3 h, one singlet every 5 h, one doublet every 11 h and one triplet every 20 h. This is the first time that triplets are unambiguously and repeatedly detected in an accreting neutron star. The bursts from all the triplets are shown in Fig. 4 together with the bursts from one singlet and from one doublet.

To reliably compare all the bursts despite the fact that many of them occur during dipping (Fig. A.1), unless otherwise stated, we base the bulk of our analysis on the hard 5−10 keV energy band because it is much less contaminated by the dipping activity than the soft band (cf. Sect. 3, Díaz Trigo et al. 2006). In addition, in Sect. 4.6.2, we perform a spectral analysis in the full 0.1−10 keV band of a sample of bursts that are the least affected by dipping, from which we derive conversion factors that we use to convert the 5−10 keV parameters values into bolometric ones in the rest of the analysis. Bursts 26 and 38 contain data gaps and are excluded from part of the analysis.

4.1. Parameters definition

Prior to each burst, we select a reference interval free of eclipse, instrumental data gaps or other bursts, in the 1-s resolution light curve. We define the burst start time when the count rate reaches 3σ above the level in the reference segment, as the burst rises,

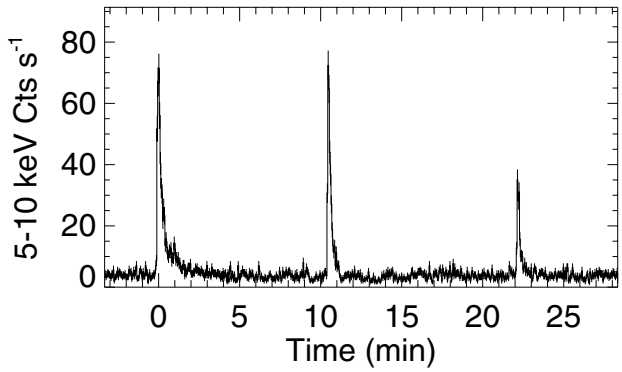

Fig. 3. 5–10 keV EPIC PN light curve of EXO 0748-676 with a binning of 3 s showing the triplet of bursts 13, 14 and 15. Time is given in minutes from the peak time of the burst 13.

and the burst stop time when the intensity drops back to a level of 1.1 times the mean intensity in the reference segment, as the burst decays. We define the burst duration as the separation between these burst stop and start times. The peak time is the time at which the count rate is maximum, again in the 1-s resolution 5−10 keV light curve. We define *the wait time* of a burst as the separation between its peak time and the peak time of the previous burst. We take *the event wait time to the next event* as the separation between the peak time of the first burst in the event to the peak time of the first burst in the following event.

We determine the total net counts in a burst by summing all the counts detected between the burst start and stop times and subtracting from this value an estimate of the number of persistent-emission counts that were emitted over the burst duration (average persistent count rate in the reference segment multiplied by the burst duration). The net counts in a burst is a tracer of the burst fluence. We define the net counts in the event (tracer of the event fluence) as the sum of the net counts of each burst in the event.

We apply a multiplicative factor of 8.1×10^{-11} erg cm^{-2} count^{-1} to convert the 5−10 keV net counts into the bolometric fluence, and a factor of 8.2×10^{-11} erg cm^{-2} count^{-1} to convert the 5−10 keV peak count rate into the bolometric peak flux (see details in Sect. 4.6.2).

The α value of a burst is defined as $f_{\rm p} \times t_{\rm wait}/E_{\rm b}$, where $f_{\rm p}$ is the bolometric persistent flux, $t_{\rm wait}$ the burst wait time and $E_{\rm b}$ the bolometric burst fluence. As the persistent flux depends on the accretion rate, the product $f_{\rm p} \times t_{\rm wait}$ is a tracer of the mass

Table 2. Mean, minimum and maximum values of the burst peak flux, duration, fluence and α value, for each burst type, derived from the 1 s resolution EPIC PN 5–10 keV light curve, assuming a conversion factor of 8.1×10^{-11} erg cm^{-2} count^{-1} between the 5–10 keV net number of counts and the bolometric burst fluence, a conversion factor of 8.2×10^{-11} erg cm^{-2} count^{-1} between the 5–10 keV peak count rate and the bolometric burst peak flux (Sect. 4.6.2) and a bolometric persistent flux of 8.44×10^{-10} erg cm^{-2} s^{-1} (Sect. 3).

Type	$t_{\rm wait}$ (h or min)			Peak flux (10^{-9} erg cm^{-2} s^{-1})			Duration (s)			Fluence (10^{-7} erg cm^{-2})			α		
	Mean	Min	Max	Mean	Min	Max	Mean	Min	Max	Mean	Min	Max	Mean	Min	Max
S1	3.20 h	2.23 h	4.64 h	7.2	5.5	11	116	55	177	1.9	0.90	3.1	53	42	102
D1	2.87 h	2.04 h	3.70 h	7.0	6.1	8.6	100	65	156	1.7	1.1	2.2	52	45	61
T1	2.46 h	2.23 h	2.79 h	6.9	6.4	7.5	81	61	94	1.4	1.2	1.6	54	49	57
S1, D1, T1	3.02 h	2.04 h	4.64 h	7.2	5.5	11	109	55	177	1.8	0.90	3.1	53	42	102
D2	13.20 min	8.40 min	19.02 min	4.7	1.7	7.5	39	22	53	0.61	0.26	1.1	12	6	17
T2	12.18 min	9.42 min	15.36 min	5.2	3.2	7.9	50	28	116	0.73	0.38	1.5	10	5	16
T3	11.70 min	10.62 min	13.02 min	2.9	1.6	6.3	23	15	42	0.30	0.091	0.87	35	8	63
D2, T2, T3	12.66 min	8.40 min	19.02 min	4.5	1.6	7.9	38	15	116	0.57	0.091	1.5	16	5	63
All types	2.05 h	8.40 min	4.64 h	6.3	1.6	11	86	15	177	1.4	0.091	3.1	40	5	102

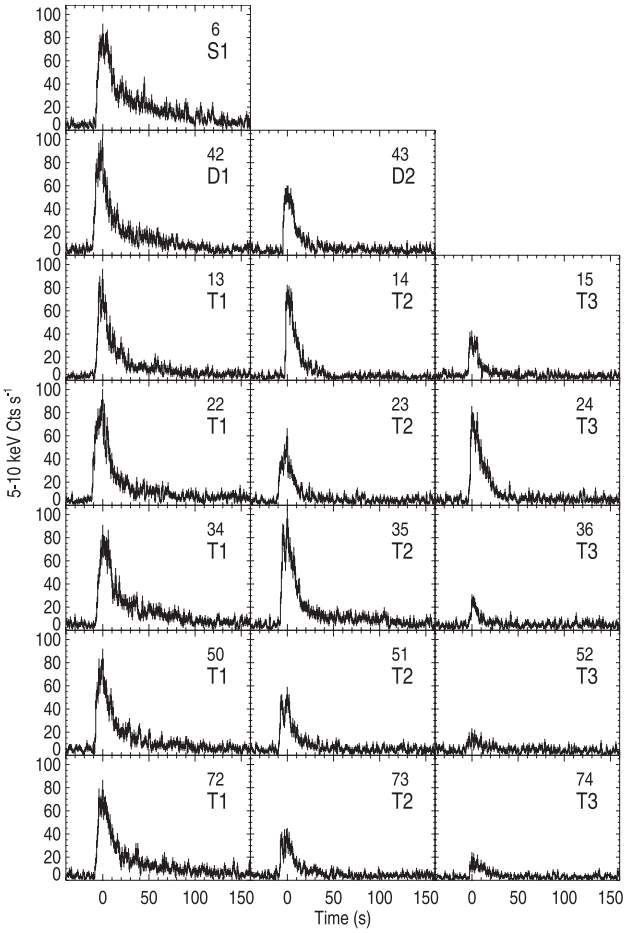

Fig. 4. 5–10 keV EPIC PN light curves of EXO 0748-676 with a binning of 1 s showing the bursts profiles in one singlet, in one doublet and in all of the five detected triplets. The burst number and its type are indicated in each panel. Time is given in seconds from the burst peak time.

accumulated on the neutron star via accretion between the preceding burst and the considered one. In the context of thermonuclear flash models, the burst fluence is expected to be proportional to the amount of nuclear fuel available. At accretion rates where the fuel does not burn stably outside bursts, the burst fluence is thus expected to be proportional to the accumulated mass, and α to be constant, in a given bursting thermonuclear regime. Here, we determine the α values assuming a constant bolometric persistent flux of 8.44×10^{-10} erg cm^{-2} s^{-1} (Sect. 3).

4.2. Parameters distributions

The peak time, wait time and type of all the bursts are listed in Table A.1. The mean, minimum and maximum values of the burst wait time, peak flux, duration, fluence and α are given in Table 2 for each burst type and for some combinations of types.

Where relevant, we indicate the skewness and kurtosis of the samples. The skewness of a sample $Y_1, Y_2, \ldots, Y_N$ is defined as $\sum_{i=1}^{N}(Y_i - \bar{Y})^3/(N-1)s^3$, where $\bar{Y}$ is the mean, s the standard deviation, and N the number of data points. The skewness is expected to be 0 for a symmetric distribution, <0 for a skewed left one, and >0 for a skewed right one. The kurtosis, defined as $[\sum_{i=1}^{N}(Y_i - \bar{Y})^4/(N-1)s^4] - 3$, is expected to be 0 for a normal distribution, <0 for a flatter one, and >0 for a more peaked one.

We use the two-sample Kolmogorov-Smirnov test to estimate the probability, $P_{\rm same}^{\rm a-b}$, that two samples a and b come from the same distribution. Since there are only 5 triplets (as compared to 14 doublets and 33 singlets), the probabilities involving the triplets are inferred from particularly small numbers and should be considered with care.

4.2.1. Wait time

The histograms of the wait times are shown in Fig. 5 for each burst type and for some combinations of burst types. The wait times range between 8.4 min and 4.6 h, but we observe no burst with a wait time between 20 min and 2 h. Two distinct groups of bursts are thus clearly visible: one group made up of the S1, D1 and T1 bursts which occur after a mean wait time of 3.0 h, and another group consisting of the D2, T2 and T3 bursts which occur after a mean wait time of only 12.7 min. We will refer to these two groups as the bursts with long wait times (LWT) and short wait times (SWT), respectively. This distinction is confirmed by the very low probability ($P_{\rm same}^{\rm long-short} = 7 \times 10^{-14}$) that the wait times from the two groups come from the same distribution. The SWT histogram and the LWT histogram have the same skewness of 0.64, and a similar kurtosis of −0.57 for the LWT and −0.31 for the SWT.

Inside the LWT group, the wait time distributions from two different burst types are not significantly different ($P_{\rm same}^{\rm S1-D1} = 37\%$, $P_{\rm same}^{\rm S1-T1} = 23\%$, $P_{\rm same}^{\rm D1-T1} = 25\%$). Inside the

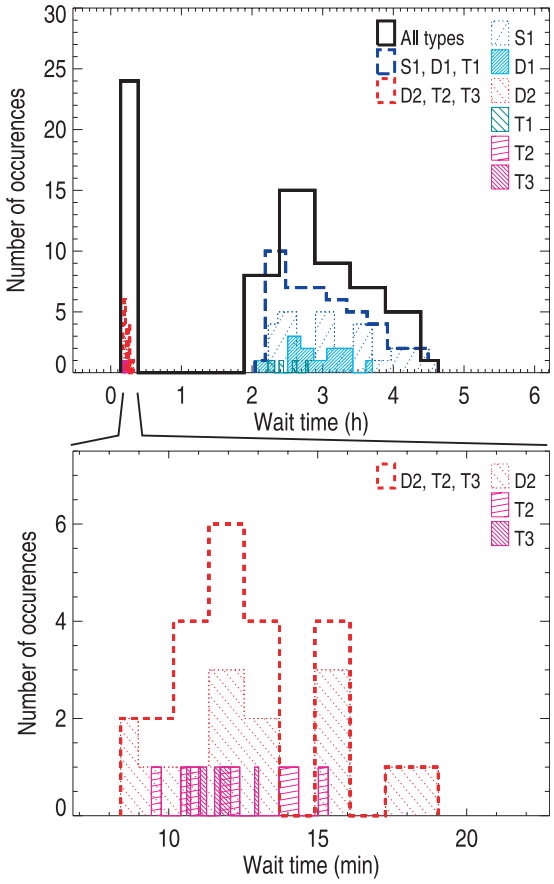

Fig. 5. Histograms of the wait times. The bottom plot zooms in on the top one. The histograms are built independently for each burst type and for some combinations of types, using always 10 bins. Consequently, the bin size is different from one histogram to another. Furthermore, the size of the first and last bins is adjusted to match the exact observed range of wait times for a given histogram.

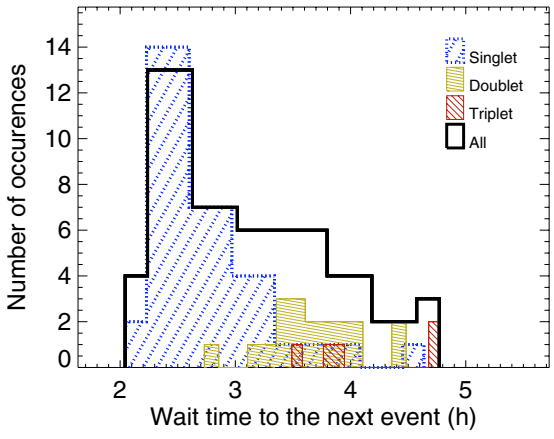

Fig. 6. Histograms of the event wait times to the next event, built independently for the singlets, doublets, triplets and for all events, using 8 bins.

SWT group, the D2, T2 and T3 bursts also seem to follow the same wait times distribution ($P_{\rm same}^{\rm D2-T2} = 96\%$, $P_{\rm same}^{\rm T2-T3} = 70\%$, $P_{\rm same}^{\rm D2-T3} = 35\%$).

Figure 6 shows the histograms of the event wait time to the next event. While the doublets and the triplets seem to follow the same distribution ($P_{\rm same}^{\rm doublet-triplet} = 58\%$), the singlets follow a significantly different distribution than that of the doublets and

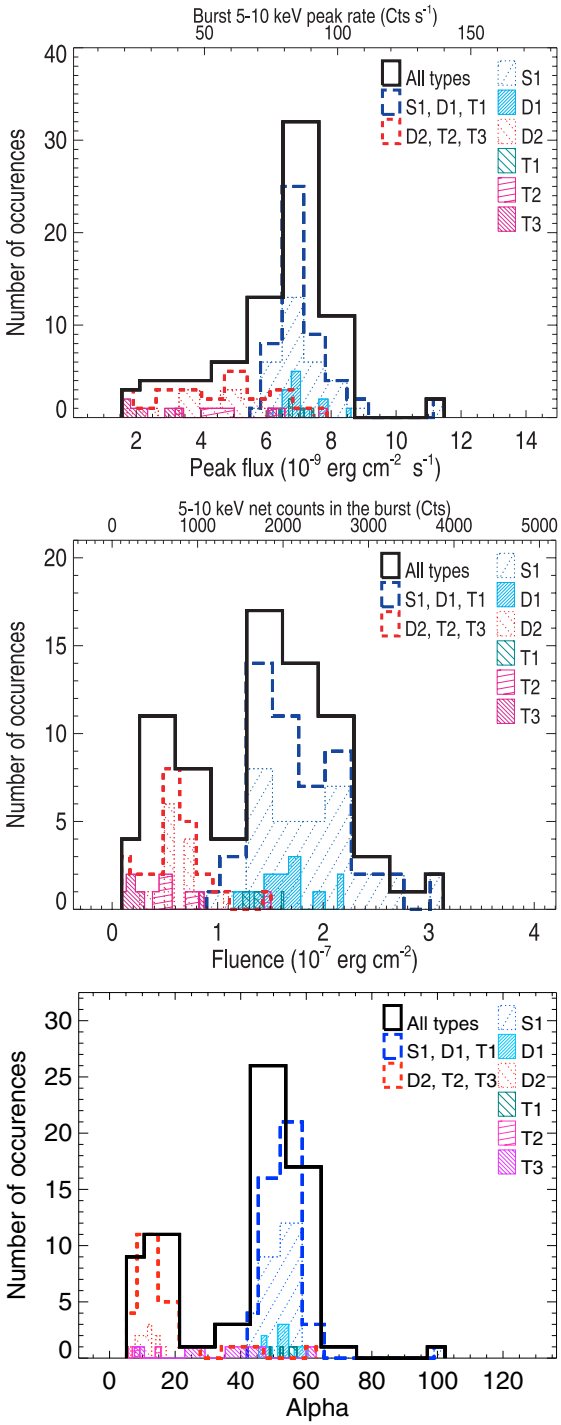

Fig. 7. Histograms of the burst peak flux (*top*), fluence (*middle*) and α values (*bottom*) built as in Fig. 5.

triplets ($P_{\rm same}^{\rm singlet-doublet} = 0.0015\%$ and $P_{\rm same}^{\rm singlet-triplet} = 0.2\%$). For a new event to occur, one has to wait on average 4.2 h after a triplet, 3.7 h after a doublet, but only 2.7 h after a singlet.

4.2.2. Peak flux

The histograms of the burst peak flux are shown in Fig. 7 (top; see also Table 2). Despite their overlap, the LWT and SWT peak flux histograms are inconsistent with coming from the same distribution ($P_{\rm same}^{\rm long-short} = 1.5 \times 10^{-8}$). The mean peak flux of the LWT bursts is a factor 1.6 higher than that of the SWT bursts.

The mean peak flux of the LWT bursts, 7.2×10^{-9} erg cm^{-2} s^{-1}, corresponds to a luminosity of 2.2×10^{37} erg s^{-1} at 5 kpc or 8.6×10^{37} erg s^{-1} at 10 kpc. The mean peak flux of the SWT bursts, 4.5×10^{-9} erg cm^{-2} s^{-1}, corresponds to a luminosity of 1.3×10^{37} erg s^{-1} at 5 kpc or 5.4×10^{37} erg s^{-1} at 10 kpc.

The LWT peak flux histogram is very peaked (kurtosis of 5.68) while that of the SWT group is flat (kurtosis of −1.06). The S1, D1 and T1 bursts have similar peak flux distributions ($P_{\rm same}^{\rm S1-D1} = 84\%$, $P_{\rm same}^{\rm S1-T1} = 96\%$, $P_{\rm same}^{\rm D1-T1} = 99\%$). In the SWT group, the D2 and T2 bursts have similar peak flux distributions ($P_{\rm same}^{\rm D2-T2} = 99\%$), while the T3 bursts seem to follow a marginally different one ($P_{\rm same}^{\rm D2-T3} = 4.5\%$, $P_{\rm same}^{\rm T2-T3} = 3.6\%$), with lower values.

In a given doublet (triplet), the peak flux of the D2 (T2) is significantly lower than that of the D1 (T1) in 10/13 (3/5) cases, and similar to it in the other cases (see Fig. 4). The peak flux of the T3 burst is always significantly less than that of the T2 burst, except for the strong T3 burst number 24.

4.2.3. Fluence and duration

The histograms of the burst fluence are shown in Fig. 7 (middle; see also Table 2). The fluence sample is clearly bimodal ($P_{\rm same}^{\rm long-short} = 7.6 \times 10^{-14}$), the SWT bursts being less fluent by a factor ∼3 than the LWT bursts on average. The mean fluence of the LWT bursts is 1.8×10^{-7} erg cm^{-2} and corresponds to 5.3×10^{38} erg at 5 kpc or 2.1×10^{39} erg at 10 kpc. The mean fluence of the SWT bursts is 5.7×10^{-8} erg cm^{-2} and corresponds to 1.7×10^{38} erg at 5 kpc or 6.8×10^{38} erg at 10 kpc.

Inside the LWT group, the fluences from the S1 and D1 bursts seem to be drawn from the same distribution ($P_{\rm same}^{\rm S1-D1} = 26\%$), while the T1 bursts would follow a marginally different one ($P_{\rm same}^{\rm S1-T1} = 4.1\%$, $P_{\rm same}^{\rm D1-T1} = 5.4\%$), the T1 being on average less fluent than the D1 or the S1 bursts. Inside the SWT group, the D2 and T2 have similar fluence distributions ($P_{\rm same}^{\rm D2-T2} = 93\%$), while the T3 have marginally different (lower) ones ($P_{\rm same}^{\rm D2-T3} = 0.7\%$, $P_{\rm same}^{\rm T2-T3} = 3.6\%$). The histograms of the burst duration (not shown here) are very similar to the fluence ones.

In a given doublet, the D2 burst is always shorter and less fluent than the D1. In a given triplet, the duration and fluence of the T2 is always less or equal to that of the T1. The T3 burst, except for the strong T3 burst number 24, has a duration and fluence less than that of the T2 burst.

4.2.4. Alpha

The histograms of the α values are shown in Fig. 7 (see also Table 2). The sample is clearly bimodal ($P_{\rm same}^{\rm long-short} = 1.0 \times 10^{-12}$), the mean α value being smaller by a factor ∼3.3 for the SWT bursts ($\alpha = 16$) than for the LWT ones ($\alpha = 53$). The α histogram for the S1 bursts is very peaked (kurtosis of 11.4) compared to all the other burst types (kurtosis between −0.4 and −2). Inside the LWT group, the S1, D1 and T1 bursts seem to follow the same α distribution ($P_{\rm same}^{\rm S1-D1} = 90\%$, $P_{\rm same}^{\rm S1-T1} = 48\%$, $P_{\rm same}^{\rm D1-T1} = 60\%$). Inside the SWT group, the T3 bursts seem to follow a marginally different α distribution from the D2 and T2 bursts ($P_{\rm same}^{\rm D2-T3} = 1.9\%$, $P_{\rm same}^{\rm T2-T3} = 3.6\%$ while $P_{\rm same}^{\rm D2-T2} = 32\%$).

Table 3. Best-fit parameters α and E_0, and their 90% confidence errors, obtained from fitting $E_{\rm b}$ as $\alpha^{-1} \times [f_{\rm p} \times t_{\rm wait}] + E_0$ (see text).

Type	α	E_0 (10^{-8} erg cm^{-2})
S1	45 ± 5	−2.5 ± 2.3
D1	49 ± 11	−1.1 ± 3.7
T1	50 ± 40	1 ± 13
S1, D1, T1	46 ± 4	−2.3 ± 1.7

4.3. Relation between burst fluence and accumulated mass

Figure 8 (left and middle panels) shows the burst fluence as a function of the product of the persistent flux times the wait time, which is a tracer of the mass accumulated by accretion before the burst. Here, the accumulated mass tracer is simply proportional to the wait time because we assume the underlying persistent flux is constant (Sect. 3).

Among the LWT types, the fluence is strongly correlated with the accumulated mass tracer, with correlation coefficients of 0.91 for the S1, 0.89 for the D1 and 0.81 for the T1 bursts. For each LWT type, the fluence is well described by a linear function of the accumulated mass tracer ($E_{\rm b} = \alpha^{-1} \times [f_{\rm p} \times t_{\rm wait}] + E_0$). E_0 is the offset energy at zero burst interval. The best-fit parameter values α and E_0 are listed in Table 3. Within the 90% confidence range, both α and E_0 are consistent with being the same for the S1, D1 and T1 bursts. For all the LWT bursts together, the α value obtained from the fit is 46 ± 4 and E_0 is $(-2.3 \pm 1.7) \times 10^{-8}$ erg cm^{-2}. E_0 is consistent with 0 within 3σ, and consistent with being negative within the 90% confidence range (1.65σ). A negative value of E_0 would indicate that a part $|E_0| = 2.3 \times 10^{-8}$ erg cm^{-2} of the total available energy is not burned in the burst. This corresponds to an energy of 6.9×10^{37} erg at 5 kpc or 2.7×10^{38} erg at 10 kpc, equivalent to 13% of the mean energy released by the LWT bursts.

Among the SWT types, only the T3 bursts show a strong correlation (coefficient of 0.86) between the fluence and the accumulated mass, which can be described by a line with best-fit parameters $\alpha = 1.2 \pm 0.4$ and $E_0 = (-4.5 \pm 4.6) \times 10^{-7}$ erg cm^{-2} (90% confidence errors). The fluence of the D2 or T2 bursts is much less strongly correlated with the accumulated mass, the coefficients being 0.53 for the D2 and 0.62 for the T2, and no acceptable linear fit could be obtained. So, apart maybe for the T3 bursts, the fluence of a SWT burst does not strongly depend on the amount of material freshly accreted just before the SWT burst.

Combining SWT and LWT types (e.g. the whole sample of bursts, or the D1 and D2 combined), we could not obtain acceptable (with reduced $\chi^2 < 2$) linear fits between the fluence and the accumulated mass tracer. Thus, the SWT bursts are inconsistent with following the same fluence- accumulated mass relation as the LWT bursts.

Figure 8 (right) shows the *event* fluence as a function of the accumulated mass tracer. At a given accumulated mass, a triplet is generally more fluent than a doublet which is more fluent than a singlet. When all the events are considered together, the event fluence is only weakly correlated to the accumulated mass tracer (correlation coefficient of 0.38). The fluence of the doublets correlates with the accumulated mass. However, this correlation is not better than the one observed for the D1 bursts only. Similarly the correlation is not improved by considering the triplets (coefficient of 0.44) rather than the T1 bursts (coefficient of 0.81). This effect is visible when the left and right panels of Fig. 8 are compared: the dispersion is higher for the doublets than for the

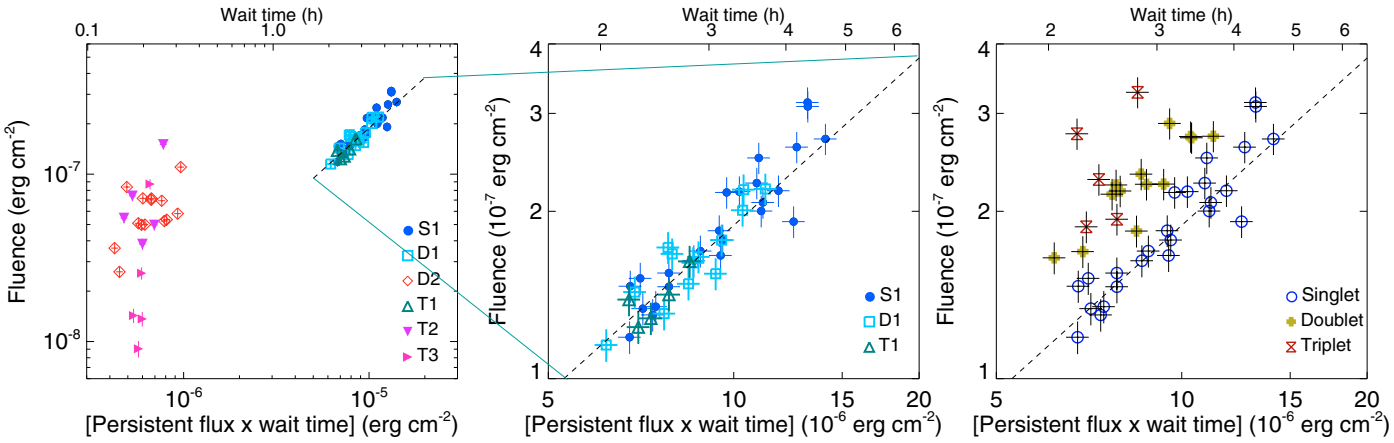

Fig. 8. *Left*: burst fluence as a function of persistent flux times wait time (accumulated mass tracer). The line indicates the mean α value for the LWT bursts ($\alpha = 53$). *Middle*: zoom in on the left panel. *Right*: event fluence as a function of the accumulated mass tracer. The line is the same as in the *left panel*.

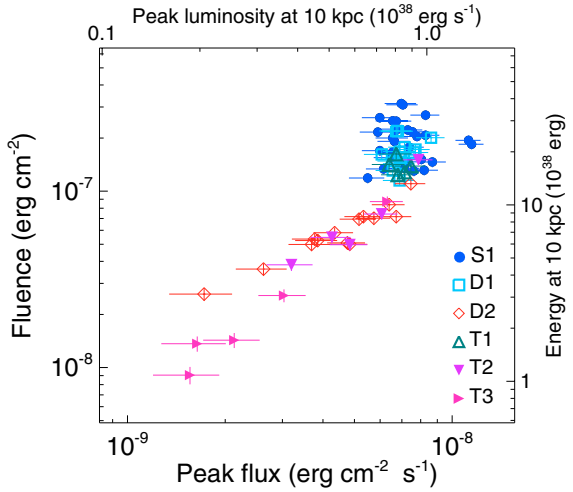

Fig. 9. Bolometric burst fluence as a function of the bolometric peak flux. The right and top axis indicate the corresponding energy and peak luminosity assuming an isotropic emission at a distance of 10 kpc.

D1 and higher for the triplets than for the T1. This suggests that the fluence of a D2 burst (and analogously of a T2-T3 pair) does not strongly depend on the amount of material accreted before the D1 (or T1) burst of the considered event.

4.4. Relation between fluence and flux

Figure 9 shows the burst fluence as a function of the burst peak flux. While the two quantities are not strongly correlated for the S1, D1 and T1 bursts (with linear correlation coefficients of 0.04, 0.29, and −0.27, respectively), the fluence and flux are strongly correlated in the case of the D2, T2 and T3 bursts, with correlation coefficients of 0.93, 0.94 and 0.99, respectively.

4.5. Profiles

Figure 10 shows the profiles obtained by averaging the 5−10 keV light curves of all the bursts of a given type, except the exceptionally strong T2 and T3 bursts number 35 and 24. After subtracting the persistent count rate level before the bursts, the decay of all these profiles is well described by a model consisting of two exponential parts. The best-fit values of the characteristic decay times, τ_1 and τ_2, and of the transition time t_1 are given in Table 4. The first part of the decay is always faster than the second ($\tau_1 < \tau_2$). The decays of the average S1, D1 and T1 profiles are similar to each other, with $\tau_1 \sim 15$ s and $\tau_2 \sim 52$ s. The D2 and T2 average profiles decay more rapidly, with both τ_1 and τ_2 being shorter. For the T3 average profile, only one exponential component is detected (including a second one does not improve the fit quality). Its decay time is similar to that of the first component of the D2 and T2 average profile.

The top panel of Fig. 11 shows the average S1, D1, T1 and D2 profiles obtained from bursts having a similar peak intensity in the range 77−96 counts s^{-1}, and a similar wait time in the range 2−2.8 h for the S1, D1 and T1. The best-fit model of their decay with two exponential parts is given in Table 5. While the S1, D1 and T1 profiles are similar, the D2 profile, *at the same peak intensity level*, shows a different and much faster decay which can be modeled by only one exponential decay.

The only T2 and T3 bursts that have a peak intensity in the range 77−96 counts s^{-1} are the exceptionally strong ones number 35 and 24, respectively. The best-fit model of their decay is given in Table 5. The decay of the strong T2 burst number 35 shows a fast part followed by a slow flat component. Interestingly, the decay of the strong T3 burst (bottom panel of Fig. 11) is very similar to that of the average D2 profile *at the same peak intensity level*.

4.6. Spectral properties

4.6.1. Color intensity diagram

Figure 12 shows the color, C, as a function of the hard intensity, I, during the decay of the averaged profiles obtained, respectively, from 15 S1, 8 D1, 10 D2, 2 T1, 1 T2 and 1 T3 bursts chosen for being the least contaminated by the dipping activity. We find that, for each burst type, $\log(C)$ can be described by a linear function of $\log(I)$ ($\log(C) = a \times \log(I) + b$). For a burst emitting like a blackbody, the bolometric flux F is expected to depend only on the area, A, of the emitting region and on the blackbody temperature, T, as $F \propto AT^4$. Since C is a tracer of T and I is a tracer of F, any difference in the slope a between burst types would indicate a difference in the flux to temperature dependence ($F \propto T^4$), while any difference in the intercept b would indicate a difference in the area A of the emitting region. We find that, within 3σ, the slope a is consistent with being the same for

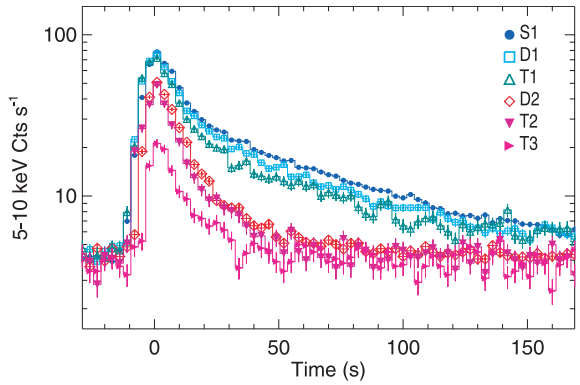

Fig. 10. Average profiles for each burst type, obtained respectively from 32 S1, 13 D1, 14 D2, 5 T1, 4 T2 and 4 T3 bursts. The strong T2 and T3 bursts number 35 and 24 are excluded. The binning is 3 s. Note that the logarithmic scale of the intensity axis makes an exponential decay appear as a straight line.

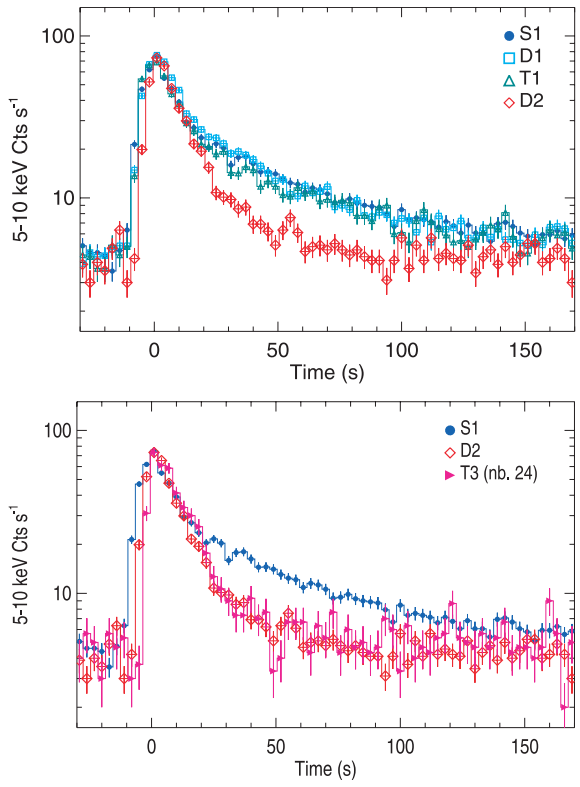

Fig. 11. *Top*: average S1, D1, T1 and D2 profiles, obtained respectively from 5 S1, 5 D1, 3 T1 and 3 D2 bursts having a similar peak intensity (77–96 counts s^{-1}), and a similar wait time for the S1, D1 and T1 (2–2.8 h). Time is given from the burst peak time and the binning is 3 s. *Bottom*: the strong T3 number 24 compared with the S1 and D2 average profiles from the top panel.

all burst types. So the comparison of the averaged color-intensity diagrams by burst types does not indicate differences by type in the burst temperature to flux dependence. The best-fit values of the intercept b are consistent with being the same within 3σ for the S1, D1, T1, T2 and T3 types on one hand, and for S1, D1, D2, T2 and T3 types on the other hand, indicating a difference only between the T1 and D2 types. This difference suggests that the apparent emitting area (or blackbody radius) would be on average larger for the T1 than for the D2 bursts.

Table 4. Best-fit parameter values and 90% confidence errors for the decay of the average profiles by burst type (Fig. 10). We subtract the persistent count rate level before the burst and fit each persistent-subtracted burst decay using a continuous function of two exponential parts: $B_0 e^{-t/\tau_1}$ between t_0 and t_1, and $B_1 e^{-t/\tau_2}$ between t_1 and t_2. We set t_0 to the burst peak time (0 s), t_2 to the first time where the persistent-subtracted intensity, B, reaches a level of 0, and B_1 to $B_0 e^{(-t_1/\tau_1)}$. The free parameters are the persistent-subtracted intensity, B_0, at the burst peak time, the characteristic decay times, τ_1 and τ_2, and the transition time t_1. We indicate the time, $t_{\rm stop}$, where the intensity, I, reaches back a level of 1.1 times the level before the burst. For the profiles whose fit was not improved by including a second exponential component, we give only the decay time of the first and only exponential component.

Type	B_0 (counts s^{-1})	τ_1 (s)	τ_2 (s)	t_1 (s)	$t_{\rm stop}$ (s)
S1	$79.7^{+1.7}_{-0.5}$	$16.2^{+0.4}_{-0.1}$	$56.9^{+2.1}_{-0.6}$	$20.7^{+0.2}_{-0.7}$	180
D1	$74.1^{+3.0}_{-0.8}$	$15.9^{+0.6}_{-0.2}$	51^{+4}_{-1}	$21.6^{+0.4}_{-1.5}$	126
T1	$71.1^{+4.8}_{-1.5}$	$13.8^{+1.0}_{-0.3}$	48^{+12}_{-2}	$20.6^{+0.6}_{-2.3}$	103
D2	$53.9^{+2.2}_{-1.5}$	$11.0^{+0.6}_{-0.2}$	19^{+13}_{-2}	25^{+2}_{-5}	52
T2	$50.5^{+4.6}_{-2.7}$	$9.0^{+1.1}_{-0.4}$	14^{+10}_{-1}	15^{+3}_{-5}	45
T3	$17.3^{+8.2}_{-0.4}$	$10.8^{+8.7}_{-0.2}$	–	–	33

Table 5. Same as Table 4 for the average profiles by type from bursts having a peak intensity in the range 77–96 counts s^{-1} and a wait time in the range 2–2.8 h for the S1, D1 and T1 (Fig. 11).

Type	B_0 (counts s^{-1})	τ_1 (s)	τ_2 (s)	t_1 (s)	$t_{\rm stop}$ (s)
S1	70^{+5}_{-1}	$14.0^{+1.1}_{-0.2}$	49^{+10}_{-2}	$19.9^{+0.5}_{-2.6}$	116
D1	81^{+6}_{-1}	$14.2^{+1.2}_{-0.2}$	40^{+8}_{-1}	$20.3^{+0.5}_{-3.0}$	105
T1	68^{+8}_{-2}	$13.7^{+1.9}_{-0.2}$	45^{+24}_{-2}	$21.0^{+0.6}_{-4.6}$	101
D2	75^{+10}_{-1}	$11.6^{+1.5}_{-0.2}$	–	–	50
T2	78^{+22}_{-2}	$13.0^{+3.5}_{-0.2}$	$149^{<-277\ a}_{-18}$	$30.7^{+0.6}_{-9.0}$	108
T3	92^{+8}_{-6}	$10.8^{+2.3}_{-0.3}$	–	–	37

[a] The second component of this decay is effectively flat, which shows in our fits as a long positive or negative exponential decay time.

Figure 13 shows the color at the burst peak as a function of the intensity at the peak, for the individual bursts the least affected by dipping activity. The two quantities are strongly correlated. This implies that the peak temperature distributions have similar properties as the peak fluxes distributions shown in Fig. 7, with a clear distinction between the SWT and the LWT bursts, the latter having higher and less variable peak temperatures. In addition, the correlation in Fig. 13 is consistent with that obtained from the averaged decays (Fig. 12). So the relation between the temperature and the flux is consistent with being the same for all burst types and for any time of the burst decay including at the peak.

This analysis shows that there is no indication for strong spectral differences between the various burst types, the flux or apparent emitting area being approximately the same at a given temperature during the decay. There is however marginal evidence that the apparent emitting area is on average larger for the first bursts in triplets than for the second bursts in doublets. This could point to differences in the structure or composition of the neutron star atmosphere/outer layers (see Sect. 5 and the discussion in Gottwald et al. 1987).

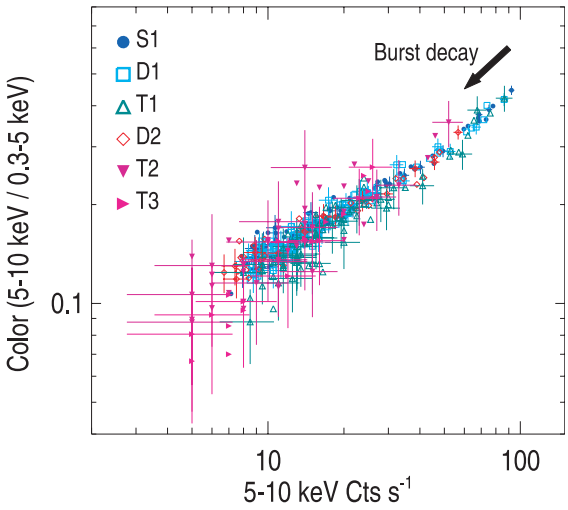

Fig. 12. Color as a function of hard intensity during the decay of the averaged profiles by type obtained, respectively, from 15 S1, 8 D1, 10 D2, 2 T1, 1 T2 and 1 T3 bursts which are the least affected by the dipping activity. Error bars are shown on one third of the points which represent each 1 s.

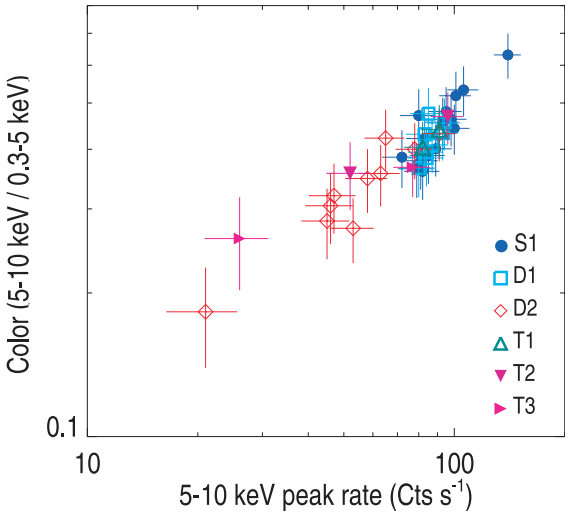

Fig. 13. Color as a function of the hard intensity at the burst peak for the individual bursts the least affected by dipping activity.

4.6.2. Time-resolved spectral modeling

We select five singlets (bursts 1, 12, 16, 33 and 37, see Appendix), one doublet (bursts 4 and 5) and two triplets (bursts 22, 23, 24 and 34, 35, 36) that are the least contaminated by dipping activity and perform their time-resolved spectral analysis using version 11.3.1 of the XSPEC package. We divide each burst into 3 to 6 intervals, with the interval around the burst peak chosen shorter than intervals in the tail. We extract a spectrum in each burst interval from which we subtract a reference persistent spectrum obtained from segments just before and after the burst. We add a 2% systematic error to account for calibration uncertainties.

Since the net emission of type-I X-ray bursts is generally well described by a blackbody (see e.g. Swank et al. 1977; Lewin et al. 1993), we model the net 0.1−10 keV spectrum with an absorbed blackbody. We fix the hydrogen column density, $N_{\rm H}$, of the neutral absorber to 0.1×10^{22} cm^{-2} (Sidoli et al. 2005). We also include a Gaussian with a centroid energy set to 0 to describe emission below ∼2 keV which is in excess of the blackbody model. This soft excess may be related to a temporary increase, due to the burst irradiation, of the ionization level of the local absorbing material in the line-of-sight. The material becomes more transparent, especially at low energy, than it was just before the burst. Consequently, the subtraction of the spectrum extracted prior to the burst from the spectrum extracted during the burst yields to an apparent soft excess in the net spectrum. This component will not be investigated further here. A soft excess was reported in other bursts from EXO 0748-676 and interpreted in a similar way by Asai & Dotani (2006).

We obtain good fits for each interval. Figure 14 (left) shows the derived blackbody temperatures and bolometric fluxes as a function of time. Figure 14 (right) shows the blackbody radius (top) and the bolometric flux (bottom) as a function of the blackbody temperature. For a given burst, we average the best-fit parameter values over the intervals near the peak on one hand, and over the intervals in the tail on the other hand. In Table 6, we give the range of these peak and tail values covered by our burst sample. The blackbody surface temperature $kT_{\rm bb}$ lies in the interval $(0.93-2.13) \pm 0.11$ keV, where higher values are found in the burst peak and lower values in the burst tail. There is no evidence for photospheric expansion. The normalization of the blackbody component and hence the radius of the emitting region is consistent with being constant throughout a burst and consistent with being the same for all the bursts studied. The average radius of the blackbody component is 2.4 km assuming a source distance of 5 kpc, and 4.9 km assuming a distance of 10 kpc, with an average uncertainty of 44%. This blackbody radius, since derived from a measured color temperature rather than the effective temperature, is an underestimate of the physical radius of the neutron star (e.g. London et al. 1984).

Using the previous spectral models, we further calculate the unabsorbed bolometric flux of the blackbody component for each interval, and finally the bolometric burst fluence by integrating over the whole burst. We find that, for our sample of bursts, the bolometric fluence linearly correlates with the 5−10 keV net counts in the burst. This means that the ratio between the bolometric fluence and the 5−10 keV net counts in the burst is consistent with being the same for all bursts types. We derive a value of $(8.1 \pm 0.3) \times 10^{-11}$ erg cm^{-2} count^{-1} for this ratio. Analogously we find a ratio of $(8.2 \pm 0.3) \times 10^{-11}$ erg cm^{-2} count^{-1} between the bolometric burst peak flux and the 5−10 keV peak count rate. These ratios serve to estimate the bolometric fluence and peak flux from the 5−10 keV counts for all other bursts, even when they are contaminated by dipping.

5. Comparison with the EXOSAT observations

In 1985, EXOSAT observed EXO 0748-676 at different persistent 0.1−20 keV fluxes between 3 and 18×10^{-10} erg cm^{-2} s^{-1} (Parmar et al. 1986; Gottwald et al. 1986). 26 bursts were observed, including four doublets with a burst separation of the order of 10−20 min (Gottwald et al. 1986). The doublet phenomenon only occurred when the persistent 0.1−20 keV flux was below 5×10^{-10} erg cm^{-2} s^{-1}, and was part of an overall correlation of the burst properties with changing mass accretion rate. As the persistent flux increased, (i) the wait time of the LWT bursts increased from ∼1.8 up to 16 h; (ii) their shape changed from a "slow" (long tail) to a "fast" profile sometimes showing photospheric expansion; (iii) their flux at a given temperature increased; and equivalently (iv) their apparent blackbody radius at a given temperature increased. Gottwald et al. (1986) hypothesized that the persistent flux dependent variations in the burst properties could be caused by the flashes changing from

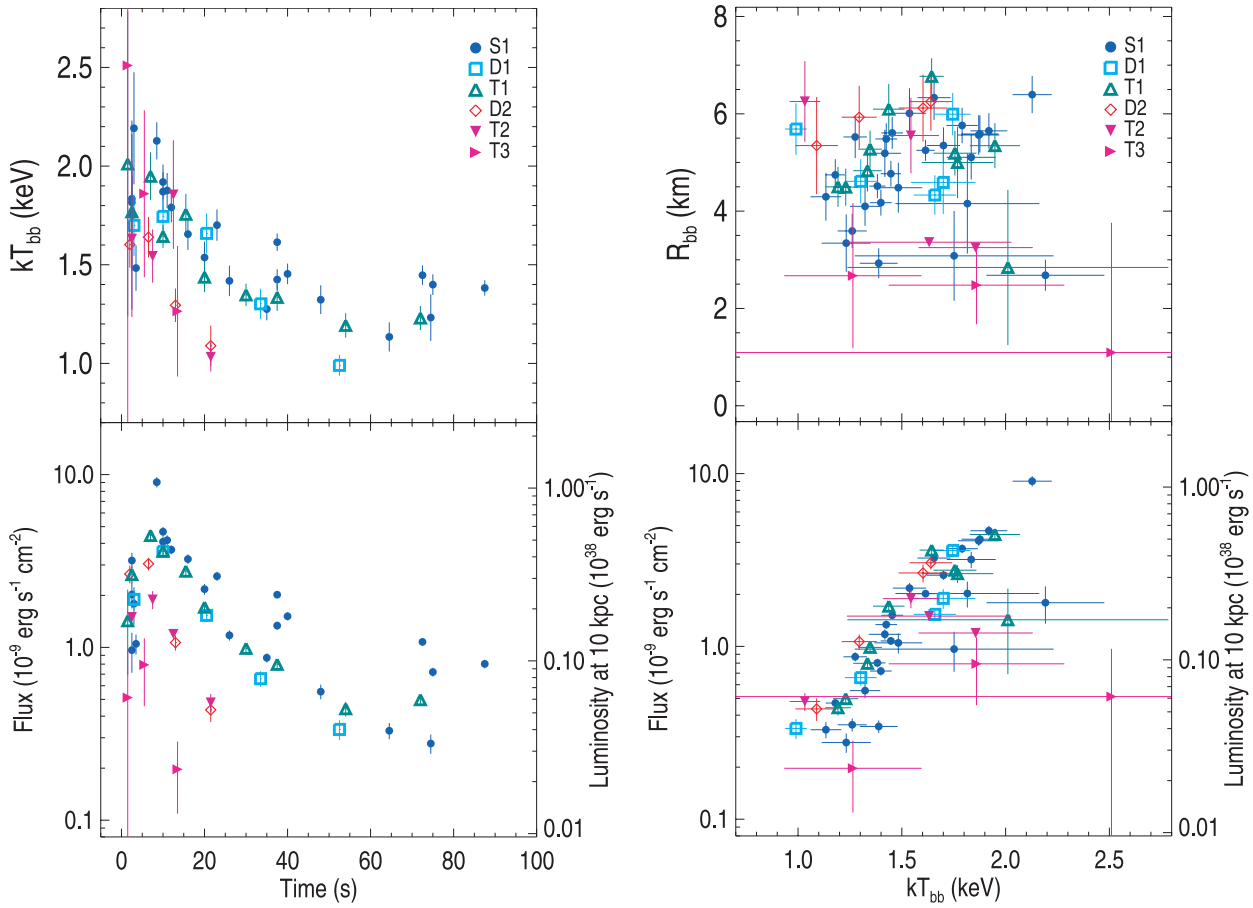

Fig. 14. Results of the time-resolved spectral analysis of bursts number 1, 12, 16, 33 and 37 (S1), 4 (D1), 5 (D2), 22 and 34 (T1), 23 (T2), and 36 (T3). *Left*: blackbody temperature (*top*) and bolometric flux (*bottom*) as a function of the time since burst onset. *Right*: blackbody radius (*top*) and bolometric flux (*bottom*) as a function of the blackbody temperature.

helium-dominated at high accretion rates, to hydrogen-triggered hydrogen-helium flashes at low accretion rates. They further speculated that double bursts could be a feature of hydrogen-triggered hydrogen-helium flashes.

In 1986, EXOSAT caught EXO 0748-676 at a persistent 0.1−20 keV flux of 5×10^{-10} erg cm^{-2} s^{-1} (Gottwald et al. 1987). 11 bursts were observed and showed a regular pattern with a long recurrence time always followed by a short one, reminiscent of the double burst phenomenon, but with longer wait times, in the range 20−70 min for the D2-like bursts. All the burst properties were otherwise consistent with that of bursts in the slow mode (i.e. low states) of 1985.

Using the spectral model by Díaz Trigo et al. (2006) (see Sect. 3), we derive an unabsorbed flux of 4.7×10^{-10} erg cm^{-2} s^{-1} in the 0.1−20 keV band for EXO 0748-676 during the 2003 XMM-Newton observations, indicating that the LMXB was again in a low state. We further suggest that the source state in 2003 is likely closer to the lowest states of 1985 than to the low state of 1986 since the unabsorbed EXOSAT fluxes are probably underestimated compared to the XMM-Newton ones because of the local neutral and ionized absorbers included in the XMM-Newton spectral models.

The comparison of Fig. 14 with Figs. 6 and 7 of Gottwald et al. (1986) and Figs. 4 and 5 of Gottwald et al. (1987) indicates that the spectral properties of the XMM-Newton bursts are all consistent with that of EXOSAT bursts in the slow mode (low states). In particular, the XMM-Newton values of the blackbody radius (4.9 ± 2.1 km on averaged) agree well with the EXOSAT values obtained in the low states whereas larger radii of ∼9 km had been obtained in higher states. These variations in the blackbody radius for a given temperature are more likely related to a change in the structure and composition of the neutron star outer layers or atmosphere which distorts the blackbody spectrum than to real variations of the emitting area (Gottwald et al. 1987). In any case, the blackbody radius, since derived from a measured color temperature rather than the effective temperature, is an underestimate of the physical radius of the neutron star (e.g. London et al. 1984). The latter one was estimated by Özel (2006) to be 13.8 ± 1.8 km in EXO 0748-676.

Figure 15 (top) shows the EXOSAT burst wait time distributions together with the XMM-Newton one. While no burst at all was detected with a wait time between ∼20 min and ∼2 h neither in 1985 nor in 2003, this gap was partly filled in 1986 by the D2-like bursts with 20−70 min wait times. Figure 15 (bottom) displays the EXOSAT wait time distributions as a function of the persistent 0.1−20 keV flux. There is a global shift of the histograms towards higher wait times as the persistent flux increases. The XMM-Newton wait time distribution, and especially the presence of doublets with ∼12 min burst separation, is consistent with that obtained by EXOSAT when EXO 0748-676 was in its lowest state in 1985.

These comparisons confirm the above-mentioned dependencies of the LWT bursts properties (shape, spectral characteristics, wait times) on the persistent flux. The presence of SWT bursts could also depend on the persistent flux in the following scheme. At low persistent flux (in the low states of 1985

Table 6. Averaged results of fits of the 0.1–10 keV spectra extracted during intervals of 13 bursts, with a model consisting of an absorbed blackbody and a Gaussian. The parameters are the hydrogen column density $N_{\rm H}$, the blackbody temperature $kT_{\rm bb}$ and normalization $N_{\rm bb}$ (defined as $R^2_{\rm km}/d^2_{10}$ where $R_{\rm km}$ is the source radius in km and d_{10} the distance to the source in units of 10 kpc), the Gaussian centroid energy E, width σ and normalization $N_{\rm G}$. For a given burst, we averaged the best-fit values from the intervals near the peak on one hand, and from the intervals in the tail on the other hand. A range indicates the spread in the obtained averaged values for the different bursts. Uncertainties are the average errors of the parameters at 1σ confidence level. $\chi^2_{\rm reduced}$ is calculated using 50 degrees of freedom. Its average and root mean squared are given.

	Peak	Tail
$N_{\rm H}$ (10^{22} cm^{-2})	0.1 (fixed)	0.1 (fixed)
$kT_{\rm bb}$ (keV)	(1.54−2.13) ± 0.12	(0.93−1.39) ± 0.09
$N_{\rm bb}$	(6−49) ± 5	(7−39) ± 5
E (keV)	0 (fixed)	0 (fixed)
σ (keV)	(0.5−0.8) ± 0.6	(0.40−0.84) ± 0.10
$N_{\rm G}$ (cts cm^{-2}s^{-1})	(0.15−1.94) ± 0.10	(0.08−0.36) ± 0.05
$\chi^2_{\rm reduced}$	1.1 ± 0.2	1.2 ± 0.3

and in 2003), doublets are emitted with a burst separation of ∼10−20 min. Triplets occur in that regime as well. They could have been missed by EXOSAT by chance since the satellite looked at EXO 0748-676 in the low state only 3 times ∼9 h, while XMM-Newton detected a triplet only once every 20 h. In 1986, the D2-like bursts have longer wait times of ∼20−70 min. This could be related to a slightly higher persistent flux then, although the derived fluxes in the low states of 1985, 1986 and 2003 are too close to each other to consider this link as certain. At much larger fluxes (in the intermediate and high states of 1985), there are no bursts with short wait times anymore.

6. Discussion

Our findings may be summarized as follows. XMM-Newton observed EXO 0748-676 in a low state 7 times, for an average of 22 h per observation, between September and November 2003. 76 sub-Eddington bursts were detected, either in single, double or triple events, respectively on 33, 14 and 5 occasions. The separation between two events is ∼3 h while the separation between two bursts in a doublet or a triplet is only ∼12 min. The primary bursts of different events are similar in terms of duration, peak flux and fluence. Their fluence is strongly correlated with the amount of material accreted before the burst. The profiles of these bursts show an initial fast decay and a second slower decaying component. Quite different are the secondary and tertiary bursts. They have a shorter duration, lower peak flux and lower fluence. Their fluence is not strongly correlated with the (little) amount of material accreted before the burst, except maybe for the tertiaries. The profiles of the secondary and tertiary bursts show only the fast decay and lack the second, more slowly decaying, component seen in the primaries. There is no strong spectral differences between the various burst types. At a given accumulated mass, the total fluence of a triplet is generally larger than that of a doublet which is larger than that of a singlet. For a new event to occur, one has to wait longer after a doublet or a triplet than after a singlet.

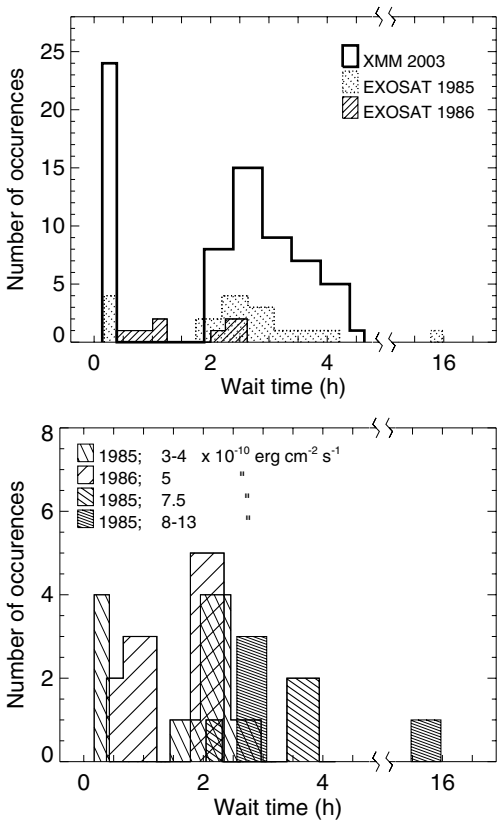

Fig. 15. *Top*: EXO 0748-676 burst wait time distributions recorded in 1985 and 1986 by EXOSAT (from Table 2 of Gottwald et al. 1986 and Table 1 of Gottwald et al. 1987) and 2003 by XMM-Newton (this paper). *Bottom*: EXOSAT burst wait time distributions as a function of the persistent 0.1–20 keV flux of EXO 0748-676 indicated in the plot (from Tables 1 and 2 of Gottwald et al. 1986). Note the broken wait time axis in both panels.

6.1. Comparison with theory: LWT bursts

How do these results fit within the current theoretical framework? Let us first consider the recurrence times and energetics of the LWT bursts. There are two ways to make bursts (or burst "events") with a recurrence time as short as 3 h: mixed H/He ignition at an accretion rate close to 10% Eddington, or unstable hydrogen ignition at an accretion rate of ≈1% Eddington.

6.1.1. Mixed H/He ignition

The best-studied of these is the first, unstable helium ignition in a hydrogen-rich environment. At high accretion rates, the accumulating fuel layer is hot enough that the hydrogen burns via the beta-limited and thermally stable hot CNO cycle (Hoyle & Fowler 1965). When the helium ignites, it burns in a hydrogen rich environment, prolonging the nuclear energy release and leads to long burst tails.

The shape of the burst lightcurves from EXO 0748-676 is similar to those observed from GS 1826-24 which Galloway et al. (2004) argued is bursting in this regime. The observed α value supports this interpretation, since the typical energy release $Q_{\rm nuc} \approx 4$ MeV per nucleon in the rp-process (e.g., Schatz et al. 1999; Table 10 of Woosley et al. 2004) gives an expected α (e.g., Galloway et al. 2004) close to the observed value $\alpha = 53$:

$$\alpha = \frac{c^2 z}{Q_{\rm nuc}}\left(\frac{\xi_{\rm b}}{\xi_{\rm p}}\right) = 48\left(\frac{z}{0.31}\right)\left(\frac{4\ {\rm MeV}}{Q_{\rm nuc}}\right)\left(\frac{\xi_{\rm p}/\xi_{\rm b}}{1.5}\right)^{-1}, \quad (1)$$

where z is the gravitational redshift, and $\xi_{b,p}$ are factors to account for anisotropy in the burst and persistent luminosities. They are defined by $L_{b,p} = 4\pi d^2 \xi_{b,p} f_{b,p}$, where $L_{b,p}$ and $f_{b,p}$ are the intrinsic luminosities and the observed fluxes, and d the distance to the source (Lapidus & Sunyaev 1985; Fujimoto 1988)[1]. $\xi_{b,p} > 1$ indicates that the observed flux is lower than it would be in the absence of anisotropy. Here we use the estimates $\xi_b^{-1} = 0.5 + |\cos i|$ and $\xi_p^{-1} = 2\,|\cos i|$, obtained by Fujimoto (1988) for a system viewed under inclination i whose geometry enhances the emission in the direction perpendicular to the disk plane, because of scattering in the disk, more strongly when the incident photons come from the inner disk (during persistent emission) than when they come from the neutron star surface (during bursts). Using $i \approx 75{-}83°$ for EXO 0748-676 (Parmar et al. 1986) gives $\xi_b \approx 1.3{-}1.6$, $\xi_p \approx 1.9{-}4.2$, and a ratio $\xi_p/\xi_b \approx 1.5{-}2.6$. We note that the $\xi_{b,p}$ estimates could significantly differ if other system geometries (e.g. including disk warping) were assumed.

In multizone X-ray burst simulations of mixed H/He ignition bursts, Woosley et al. (2004) found recurrence times close to 3 h for accretion of solar metallicity material at $\dot{M} = 1.75 \times 10^{-9}\ M_\odot\ \mathrm{yr}^{-1}$, or luminosity $\dot{M}(GM/R) \approx 2 \times 10^{37}\ \mathrm{erg\ s}^{-1}$ for a 1.4 $M_\odot$, 10 km neutron star (models zM and ZM of Woosley et al. 2004). This agrees quite well with the observed X-ray luminosity from EXO 0748-676, once the anisotropy parameter is included. The unabsorbed 0.1–100 keV flux is $8.4 \times 10^{-10}\ \mathrm{erg\ cm}^{-2}\ \mathrm{s}^{-1}$, giving a luminosity $L_X = 0.48 \times 10^{37}\ \mathrm{erg\ s}^{-1}$ ($\xi_p/1.9$) for a distance of 5 kpc and $L_X = 1.9 \times 10^{37}\ \mathrm{erg\ s}^{-1}$ ($\xi_p/1.9$) for a distance of 10 kpc, where we normalize the anisotropy parameter to $i = 75°$. Therefore we find that the recurrence times and α values of the LWT bursts agree well with the models of Woosley et al. (2004), particularly when the anisotropy factor is included.

However, the total energies of the LWT bursts in EXO 0748-676 are somewhat lower than in the models, or than observed for GS 1826-24. In the mixed H/He regime, the ignition column depth is $y_{ign} \approx 2 \times 10^8\ \mathrm{g\ cm}^{-2}$ (Cumming & Bildsten 2000) giving a burst energy $E_{burst} = 4\pi R^2 Q_{nuc} y_{ign}/(1+z) = 7.4 \times 10^{39}$ erg (assuming complete burning of the whole surface, radius $R = 10$ km, and energy release $Q_{nuc} = 4$ MeV). This estimate agrees well with models zM and ZM of Woosley et al. (2004, see their Table 9) and with the observed burst energies in GS 1826-24 (5.3×10^{39} erg at 6 kpc, Galloway et al. 2004), while the mean burst energy for the LWT bursts in EXO 0748-676 is $(0.5{-}2.1) \times 10^{39}$ erg for the distance range 5–10 kpc. Note that anisotropy, which would tend to decrease the burst luminosity for GS 1826-24 (Galloway et al. 2004) and increase it for EXO 0748-676 (Fujimoto 1988), is not included in these estimates.

The same is true for the peak luminosity. The high base temperatures $\gtrsim 10^9$ K reached in mixed H/He bursts give a peak luminosity $\gtrsim 10^{38}\ \mathrm{erg\ s}^{-1}$ (e.g., Woosley et al. 2004), approaching the Eddington luminosity. Ignoring anisotropy, in GS 1826-24, the bursts peak flux was $3 \times 10^{-8}\ \mathrm{erg\ cm}^{-2}\ \mathrm{s}^{-1}$, giving $L_{peak} = 1.3 \times 10^{38}\ \mathrm{erg\ s}^{-1}$ at 6 kpc (Galloway et al. 2004). In contrast the mean peak flux for the LWT bursts in EXO 0748-676 is $7.2 \times 10^{-9}\ \mathrm{erg\ cm}^{-2}\ \mathrm{s}^{-1}$, giving $L_{peak} = (0.22{-}0.86) \times 10^{38}\ \mathrm{erg\ s}^{-1}$ for the distance range 5–10 kpc. Independent of the assumed distance, it is a factor of 7 below the peak flux of the bright radius expansion burst observed by Wolff et al. (2005) from EXO 0748-676, further showing that these LWT bursts are faint relative to the Eddington luminosity.

[1] We note that anisotropy of the burst luminosity was not included in the analysis by Özel (2006). The EXO 0748-676 neutron star mass and radius determinations in that paper are likely unaffected by the anisotropy factor, as long as it is constant through the burst, since they come from taking the ratio of the peak flux and the flux in the tail. However, the lower limit on the source distance, $d > 9.2 \pm 1.0$ kpc should be reduced by a factor $\xi_b^{1/2}$, or 15–30%, giving $d > 7.3$–8.1 kpc for $\xi_b = 1.3$–1.6, using the estimate of Fujimoto (1988).

6.1.2. Hydrogen ignition

The low burst energies and peak luminosities suggest a different explanation for the LWT bursts from EXO 0748-676, that they are triggered by unstable hydrogen ignition. Hydrogen burning is unstable for temperatures less than $\approx 8 \times 10^7$ K, when the CNO is no longer beta-limited, and can trigger thermonuclear flashes (Fujimoto et al. 1981).

Bildsten (1998) estimates that unstable hydrogen ignition occurs for accretion rates $\dot{M} \lesssim 2 \times 10^{-10}\ M_\odot\ \mathrm{yr}^{-1}$, or luminosities $L_X \lesssim 2 \times 10^{36}\ \mathrm{erg\ s}^{-1}$. This matches the luminosity of EXO 0748-676 if the source is located at the closer end of its distance range, and the anisotropy factor is small. The observed recurrence time of $\approx$3 h matches the recurrence time expected close to the transition between unstable and stable hydrogen burning. The maximum temperature at which hydrogen can unstably ignite, close to 8×10^7 K, corresponds to a column depth of approximately $10^7\ \mathrm{g\ cm}^{-2}$ (see Fig. 1 of Cumming 2004). At an accretion rate of 1% of the Eddington rate, this column is accreted in 3.2 h.

There are two possible outcomes of unstable hydrogen ignition (Fujimoto et al. 1981; Peng et al. 2006). If the hydrogen ignition depth is $\gtrsim 5 \times 10^7\ \mathrm{g\ cm}^{-2}$, the minimum column depth at which helium can ignite (Fig. 1 of Cumming 2004), the increase in temperature following hydrogen ignition triggers ignition of helium by the triple alpha reaction, and a mixed hydrogen/helium flash occurs. At smaller ignition depths, which occur near the transition between unstable and stable hydrogen burning, the hydrogen flash is not able to trigger helium ignition. This case has recently been modeled by Peng et al. (2006). They include, for the first time, sedimentation of heavy elements in the accumulating fuel layer. For an accretion rate close to 1% of the Eddington rate, they find that the hydrogen flash reaches a peak luminosity of 5 times the accretion luminosity, or $\approx 0.1 \times 10^{38}\ \mathrm{erg\ s}^{-1}$. This is lower than the observed peak luminosities of the LWT bursts by a factor of a few. Burning a column depth of $10^7\ \mathrm{g\ cm}^{-2}$ of hydrogen to helium gives an expected burst energy 0.6×10^{39} erg (using the energy release $Q_{nuc} = 6.0 \times 10^{18}\ \mathrm{erg\ g}^{-1}$ appropriate for the hot CNO cycle). This is within the range of observed energy for the LWT bursts.

Although the peak luminosity found by Peng et al. (2006) is a little lower than observed for the LWT bursts, they only computed a few different cases of hydrogen ignition. In addition, the recurrence time and burst energies do match the expectations for hydrogen ignition close to the stability boundary quite well. An interesting point about this interpretation is that the sedimentation of heavy elements plays a crucial role (Peng et al. 2006). Without sedimentation, the CNO abundance remains close to the solar value at the ignition depth, and the energy released by the initial proton captures is small giving a very weak flash. With sedimentation, the CNO abundance is enhanced by a factor of several, leading to more energy release during the initial runaway, giving a peak temperature of $\approx 3 \times 10^8$ K and a peak luminosity observable above the accretion luminosity.

In addition, the interpretation of the LWT bursts as hydrogen flashes also provides two explanations for the bright energetic burst ($E_b = 3.6 \times 10^{-7}\ \mathrm{erg\,cm}^{-2}$) reported by

Wolff et al. (2005) from EXO 0748-676 at a low persistent flux ($f_p = 4.8 \times 10^{-10}$ erg cm^{-2} s^{-1}). First, if the hydrogen flash fails to ignite helium, a pure helium layer builds up beneath the hydrogen burning shell which will eventually ignite by triple alpha reactions. Alternatively, since the burst properties indicate that the hydrogen ignition is occurring close to the transition between unstable and stable hydrogen burning, a slight increase in accretion rate would lead to stable hydrogen burning and a similar accumulation of a pure helium layer. Second, if the accretion rate drops, the hydrogen ignition column depth becomes large enough to trigger helium ignition resulting in a mixed H/He flash. Wolff et al. (2005) derive a burst fluence of 3.6×10^{-7} erg cm^{-2} which translates to a burst energy of $(1.5–2.5) \times 10^{39}$ erg (depending on whether the peak luminosity corresponds to the Eddington limit for solar composition or for pure helium; the corresponding distances are 5.9 and 7.7 kpc). Assuming $Q_{\rm nuc} = 1.6$ MeV, appropriate for helium burning to iron group, the implied thickness of the fuel layer is $\approx 10^8$ g cm^{-2}. A pure helium layer accumulating beneath the hydrogen shell would typically reach much greater thicknesses before igniting. Therefore, it seems likely that the Wolff et al. (2005) burst is another example of a hydrogen ignition, but this time also igniting the helium.

6.2. Comparison with theory: SWT bursts

We have spent some time discussing the origins of the LWT bursts in the hope that this might give a clue to the origin of the SWT bursts. These have so far evaded theoretical explanation, although possibilities have been put forward in the literature. Fujimoto et al. (1987) suggested that unburned fuel left over from the preceding burst is mixed downwards by hydrodynamic instabilities driven by rotational shear. Wallace & Woosley (1984) suggested that fresh fuel could be mixed downwards by Rayleigh-Taylor instabilities which set in as the layer cools. However, neither of these explanations offers a natural explanation for the ten minute delay time. This point is emphasized dramatically by the discovery of burst triplets discussed in this paper. The fact that the same characteristic timescale sets the delay between the second and third bursts in a triplet as well as the first and second points to some physical process with this timescale that can recur more than once in succession.

Mixed H/He bursts at accretion rates close to 0.1 of the Eddington rate have been modeled extensively in spherical symmetry with large nuclear reaction networks (Woosley et al. 2004). However, there has been little work on hydrogen triggered bursts, and so the suggestion that the LWT bursts are hydrogen triggered opens up the possibility that the ten minute phenomenon is connected with unstable hydrogen burning. For example, the half-life of ^{13}N in the CNO cycle is 9.97 min, very close to the observed timescale. Perhaps as the layer cools following the initial flash, an instability driven by proton captures on ^{13}C or ^{14}N occurs once there has been time for enough seed nuclei to be produced by the beta-decay of ^{13}N. However, it is not clear how the fact that the timescale between SWT bursts changes (see Sect. 5), possibly with accretion rate, would be accommodated in this picture. Further theoretical studies of hydrogen triggered bursts are needed to explore the possibility that the SWT bursting has a nuclear physics explanation.

Even without a good picture of the physics of the SWT bursts, we can explore some possibilities by considering the idea that the second and third bursts are caused by ignition of leftover fuel from the first burst. One way that this might happen is that the ignition conditions for the first burst are always the same, but that sometimes incomplete burning occurs, leaving behind unburned fuel that later reignites leading to double or triple events. However, this is inconsistent with the observation that, at a given wait time, the fluence is the same for a D1, a T1 or a S1 burst (the LWT bursts have all the same alpha values). In addition, the fact that the wait time to the next event is longer after a double or triple (regardless of the type of the next event) also suggests a different picture. Imagine that after the first burst (either S1, D1, or T1), a fraction f of the fuel layer is left unburned. Then, in double or triple events, this leftover fuel layer is burned after a delay time of $\approx$10 min, whereas in single events, the unburned fuel survives, and leads to early ignition of the next event. The difference between singles and doubles/triples here is not whether there is any unburned fuel, but instead whether the unburned fuel is able to ignite on the ten minute timescale.

One way to test this idea is to look for consistency between the wait times and the burst fluences. The wait time after a double (triple) is $\approx$37% (55%) longer than the wait time after a single, suggesting that a fraction $f_a \approx 37\%$ (55%) of the available accreted fuel is not burned during the first burst. If this unburned fuel was of the same composition as the rest of the layer and burned subsequently in the second/third bursts, we would expect the double/triple events to have a larger fluence by the same factor $f_{\rm a}$. Now, the double (triple) events have larger fluences than the singles, but only by a factor $f_{\rm b}$ of $\approx$17% (25%). This indicates that the layer that burns in the second/third bursts has a lower energy per gram, for example a smaller hydrogen content than the accreted fuel that burns in the first burst. This suggests that in fact the "unburned" fuel layer undergoes some hydrogen burning into helium during the first burst. Interestingly, the ratio $f_{\rm a}/f_{\rm b}$ is $\approx$2.2 for both the doubles and the triples and is $\lesssim$2.5 which is the value of the ratio between the energy released by an hydrogen nucleon burning to the iron group (4 MeV) and the energy released by an helium nucleon burning to the iron group (1.6 MeV). The burst lightcurves also support the idea that the second/third bursts have a smaller hydrogen fraction since they have a much shorter tail than the first bursts.

These properties would be naturally explained if the first burst in the sequence involved unstable hydrogen burning into helium. If hydrogen ignition is occurring near the transition from unstable to stable hydrogen burning, then it is not clear whether helium is burning at all in the first flash. Certainly, it is not able to ignite unstably at low column depths but maybe it burns slightly at the peak temperature. The first flash would thus leave a large part (if not all) of the available helium unburned and further produce some. A subsequent second/third burst would take place in an helium-rich environment. The fact that little material can be accreted within ten minutes suggests that the SWT bursts are also hydrogen triggered since lower column depths are required than for helium ignition. More theoretical work on hydrogen ignition bursts is needed to test these ideas.

One important question concerns the occurrence rate of quadruple events. We did not observe a quadruple burst from EXO 0748-676. Galloway et al. (2006) report one quadruple event from 4U 1636−536 in the RXTE burst catalog. The occurrence rate of quadruple versus triple events (as well as triple versus double events) could provide an important constraint on theoretical models.

Conclusion

This is the first time that unambiguously and repeatedly triple bursts are detected in an accreting neutron star, EXO 0748-676. The source was already known to frequently exhibit double

bursts, where two bursts are separated by only 12 min. Now the same time scale is seen in triple bursts. This recurrence time is too short to accrete a sufficient amount of fuel, which indicates that there must have been fuel left unburned in the previous burst. We suggest that after each burst there is an amount of fuel left unburned, which may or may not reignite after 12 min, in the former case producing a double or triple burst. We find evidence that this unburned fuel yields less energy per gram, pointing to a lower hydrogen content than for the fuel of the primary bursts.

The recurrence times of 3 h and the low alpha values are consistent with mixed hydrogen/helium burning at 0.1 Eddington, as seen for example in GS 1826-24. The persistent luminosity of EXO 0748-676 is consistent with this accretion rate if the X-ray emission from the system is anisotropic, as predicted for large inclination angles. However, the expected energies and peak luminosities are somewhat larger than observed in EXO 0748-676. In addition, this burning regime has been well-studied theoretically and does not predict the ten minute bursting phenomenon. New physics, such as mixing of fuel to deeper layers, is required to explain the multiple events within the mixed hydrogen/helium burning regime.

Hydrogen ignition at a lower accretion rate may provide a more natural explanation for the burst behavior of EXO 0748-676. Hydrogen ignition bursts are not well-studied, but the properties of the bursts from EXO 0748-676 agree quite well with the recent work by Peng et al. (2006). In particular, the low peak luminosity and burst energies of the LWT bursts, and the low persistent luminosity are consistent with burning in this regime. This opens up the exciting possibility that the ten minute recurrence time bursts are in fact a natural consequence of hydrogen ignition bursts.

Acknowledgements. This work is based on observations obtained with XMM-Newton, an ESA science mission with instruments and contributions directly funded by ESA member states and the USA (NASA). SRON is supported financially by the NWO, the Netherlands Organization for Scientific Research. A.C. would like to thank Brandon Helfield for help with understanding hydrogen ignitions, and Ed Brown for sharing results on hydrogen triggered bursts prior to publication. A.C. is an Alfred P. Sloan Research Fellow, and is grateful for support from an NSERC Discovery Grant, Le Fonds Québécois de la Recherche sur la Nature et les Technologies, and the Canadian Institute for Advanced Research.

References

Aoki, T., Dotani, T., Ebisawa, K., et al. 1992, PASJ, 44, 641
Asai, K., & Dotani, T. 2006, PASJ, 58, 587
Ayasli, S., & Joss, P. C. 1982, ApJ, 256, 637
Bildsten, L. 1998, in NATO ASIC Proc. 515: The Many Faces of Neutron Stars, ed. R. Buccheri, J. van Paradijs, & A. Alpar, 419
Cottam, J., Paerels, F., & Mendez, M. 2002, Nature, 420, 51
Cumming, A. 2004, Nucl. Phys. B Proc. Suppl., 132, 435
Cumming, A., & Bildsten, L. 2000, ApJ, 544, 453
den Herder, J. W., Brinkman, A. C., Kahn, S. M., et al. 2001, A&A, 365, L7
Díaz Trigo, M., Parmar, A. N., Boirin, L., Méndez, M., & Kaastra, J. S. 2006, A&A, 445, 179
Frank, J., King, A. R., & Lasota, J. P. 1987, A&A, 178, 137
Fujimoto, M. Y. 1988, ApJ, 324, 995
Fujimoto, M. Y., Hanawa, T., & Miyaji, S. 1981, ApJ, 247, 267
Fujimoto, M. Y., Sztajno, M., Lewin, W. H. G., & van Paradijs, J. 1987, ApJ, 319, 902
Galloway, D. K., Cumming, A., Kuulkers, E., et al. 2004, ApJ, 601, 466
Galloway, D. K., Muno, M. P., Hartman, J. M., et al. 2006, ApJS [arXiv:astro-ph/0608259]
Gottwald, M., Haberl, F., Parmar, A. N., & White, N. E. 1986, ApJ, 308, 213
Gottwald, M., Haberl, F., Parmar, A. N., & White, N. E. 1987, ApJ, 323, 575
Hoyle, F., & Fowler, W. A. 1965, in Quasi-Stellar Sources and Gravitational Collapse, ed. I. Robinson, A. Schild, & E. L. Schucking, 17
Inoue, H., Koyama, K., Makino, F., et al. 1984, PASJ, 36, 855
Jansen, F., Lumb, D., Altieri, B., et al. 2001, A&A, 365, L1
Jonker, P. G., & Nelemans, G. 2004, MNRAS, 354, 355
Langmeier, A., Sztajno, M., Hasinger, G., Truemper, J., & Gottwald, M. 1987, ApJ, 323, 288
Lapidus, I. I., & Sunyaev, R. A. 1985, MNRAS, 217, 291
Lewin, W. H. G., Hoffman, J. A., Doty, J., et al. 1976, MNRAS, 177, 83P
Lewin, W. H. G., van Paradijs, J., & Taam, R. E. 1993, Space Sci. Rev., 62, 223
London, R. A., Howard, W. M., & Taam, R. E. 1984, ApJ, 287, L27
Murakami, T., Inoue, H., Koyama, K., et al. 1980, PASJ, 32, 543
Ohashi, T., Inoue, H., Koyama, K., et al. 1982, ApJ, 258, 254
Özel, F. 2006, Nature, 441, 1115
Parmar, A. N., White, N. E., Giommi, P., & Gottwald, M. 1986, ApJ, 308, 199
Pedersen, H., Motch, C., van Paradijs, J., et al. 1982, ApJ, 263, 340
Peng, F., Brown, E. F., & Truran, J. W. 2006, ApJ, submitted
Schatz, H., Bildsten, L., Cumming, A., & Wiescher, M. 1999, ApJ, 524, 1014
Sidoli, L., Parmar, A. N., & Oosterbroek, T. 2005, A&A, 429, 291
Strüder, L., Briel, U., Dennerl, K., et al. 2001, A&A, 365, L18
Swank, J. H., Becker, R. H., Boldt, E. A., et al. 1977, ApJ, 212, L73
Turner, M. J. L., Abbey, A., Arnaud, M., et al. 2001, A&A, 365, L27
Wallace, R. K., & Woosley, S. E. 1984, in American Institute of Physics Conf. Ser., ed. S. E. Woosley, 319
Wijnands, R., Muno, M. P., Miller, J. M., et al. 2002, ApJ, 566, 1060
Wolff, M. T., Hertz, P., Wood, K. S., Ray, P. S., & Bandyopadhyay, R. M. 2002, ApJ, 575, 384
Wolff, M. T., Becker, P. A., Ray, P. S., & Wood, K. S. 2005, ApJ, 632, 1099
Woosley, S. E., Heger, A., Cumming, A., et al. 2004, ApJS, 151, 75

Online Material

Appendix A: Light curves and bursts lists

Figure A.1 shows the EPIC PN light curves of EXO 0748-676 with a binning of 60 s during XMM-Newton revolutions 692 to 719. Panels a and b show the 5−10 keV and the 0.3−5 keV energy band, respectively. Panel c shows the hardness ratio. Times are not barycentre-corrected. A cycle number tracing the eclipse timing is indicated on the top axis. This was determined from a reference time of 13.79 h on 2003 September 19 (or XMM-Newton time of $1.8036643e+08$ s) estimated as the mid-time of the first eclipse observed during revolution 692, and using an orbital period of 3.824 h (Wolff et al. 2002). Integer values of the cycle number correspond to phase 0, or estimated eclipse mid-times.

The peak time, wait time and type of all the bursts are listed in Table A.1. Since the wait time of the first burst of each observation in the series cannot be determined, a lower limit is given as the separation between the burst peak time and the start time of the observation. An upper limit is given as the separation between the burst peak time and peak time of the last burst observed during the previous observation of the series.

We note that because of scattering, residual emission is present during eclipses at a level of ∼4% of the source's persistent flux. This explains why an X-ray burst was once detected during an eclipse with EXOSAT (Gottwald et al. 1986). This implies that any S1, D1 or T1 (ie. strong) burst occurring during an eclipse of the XMM-Newton observation would have been detected. Since we do not detect any burst during eclipses, it appears unlikely that we have missed an S1, D1 or T1 burst because of eclipses. Furthermore, since an eclipse lasts ∼500 s, which is less than the typical separation of the bursts in a multiple burst event, it is not possible either to have missed a complete doublet or triplet. From the inspection of Fig. A.1, we can therefore conclude that it is unlikely that any S1, D1, T1, D2, T2 or T3 burst has been missed because of an eclipse.

However, bursts occurring close to (less than 25 min) the beginning or the end of an observation, or close to a short instrumental gap such as occasionnally present in the data, cannot have their type determined certainly because another burst of the same event could have occurred during the gap and been missed. In such cases, the different possible types are indicated in Table A.1 starting with the one attributed to the burst in this analysis.

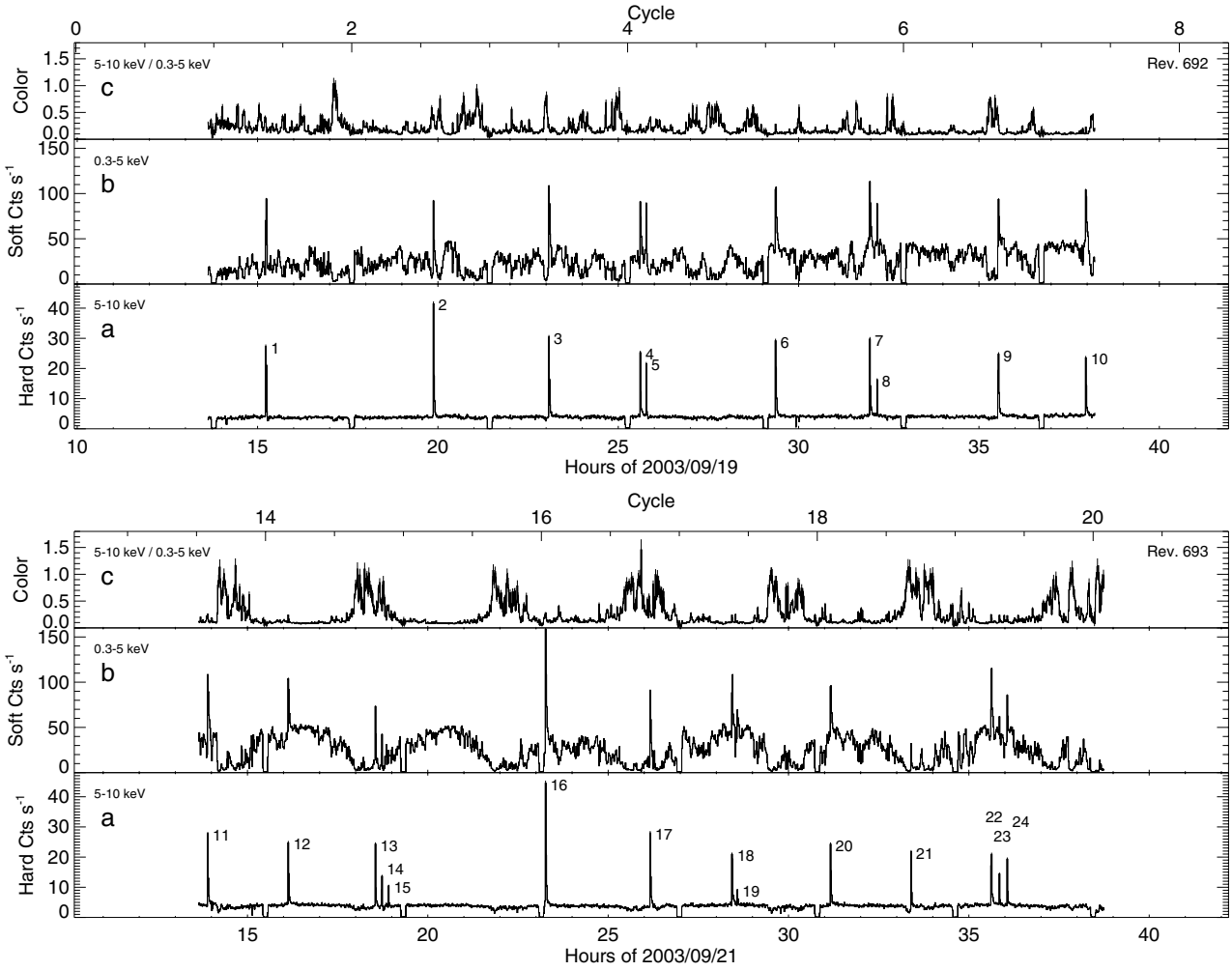

Fig. A.1. EXO 0748-676 as observed by XMM-Newton EPIC PN during revolutions 692 (*top*) and 693 (*bottom*). **a)** 5–10 keV light curve. The bursts are numbered. **b)** 0.3–5 keV light curve. **c)** Color (counts in the 5−10 keV band divided by counts in the 0.3−5 keV band) as a function of time. The binning time is 60 s in each panel. The cycle number is indicated on the top axis, with the estimated mid-eclipse time of the first eclipse observed during revolution 692 taken as cycle number 1.

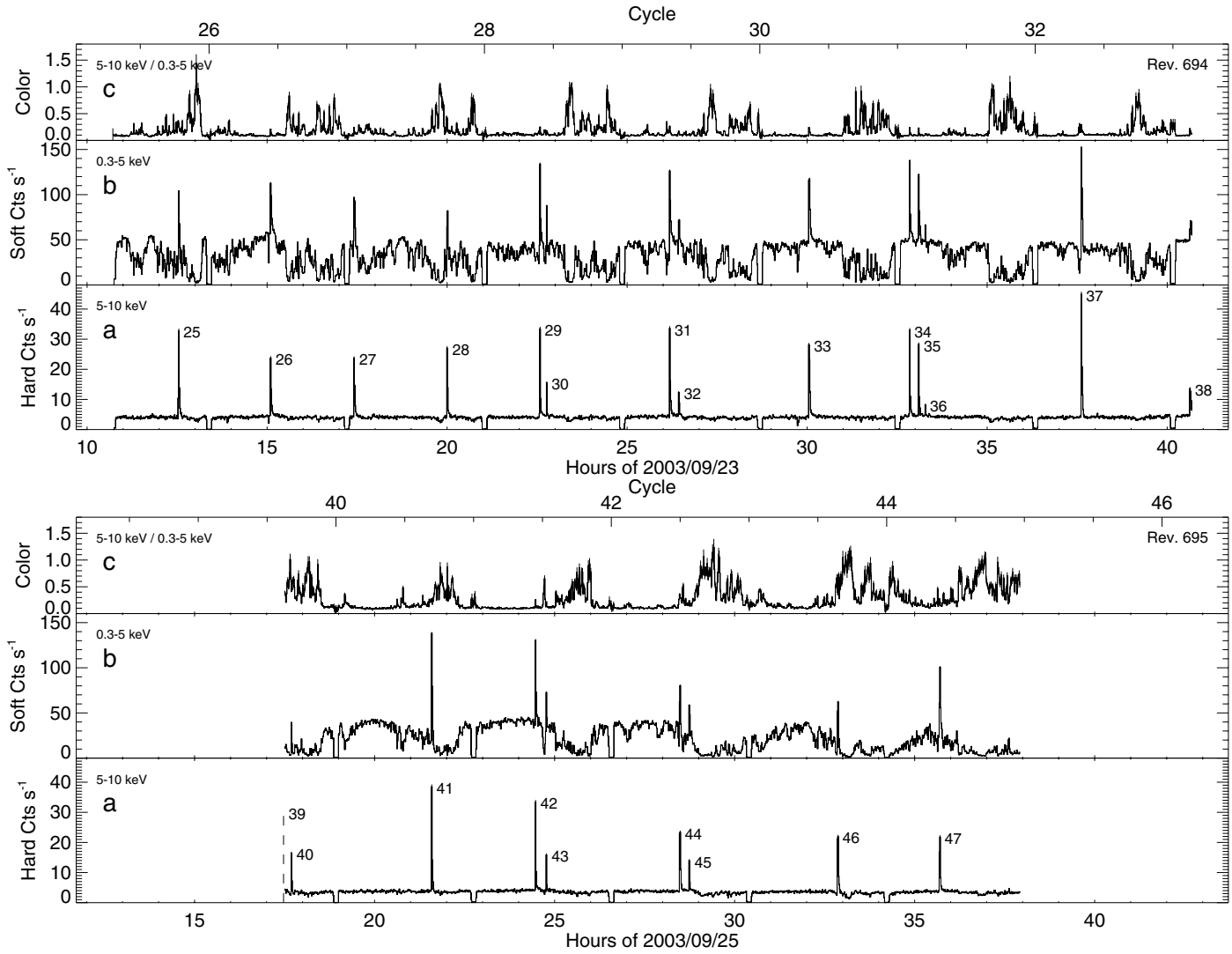

Fig. A.1. continued, for XMM-Newton revolutions 694 (*top*) and 695 (*bottom*). The dashed line in panel **c)** of the bottom plot indicates the time of a burst (numbered 39) detected by RGS just before the start of the EPIC PN observation.

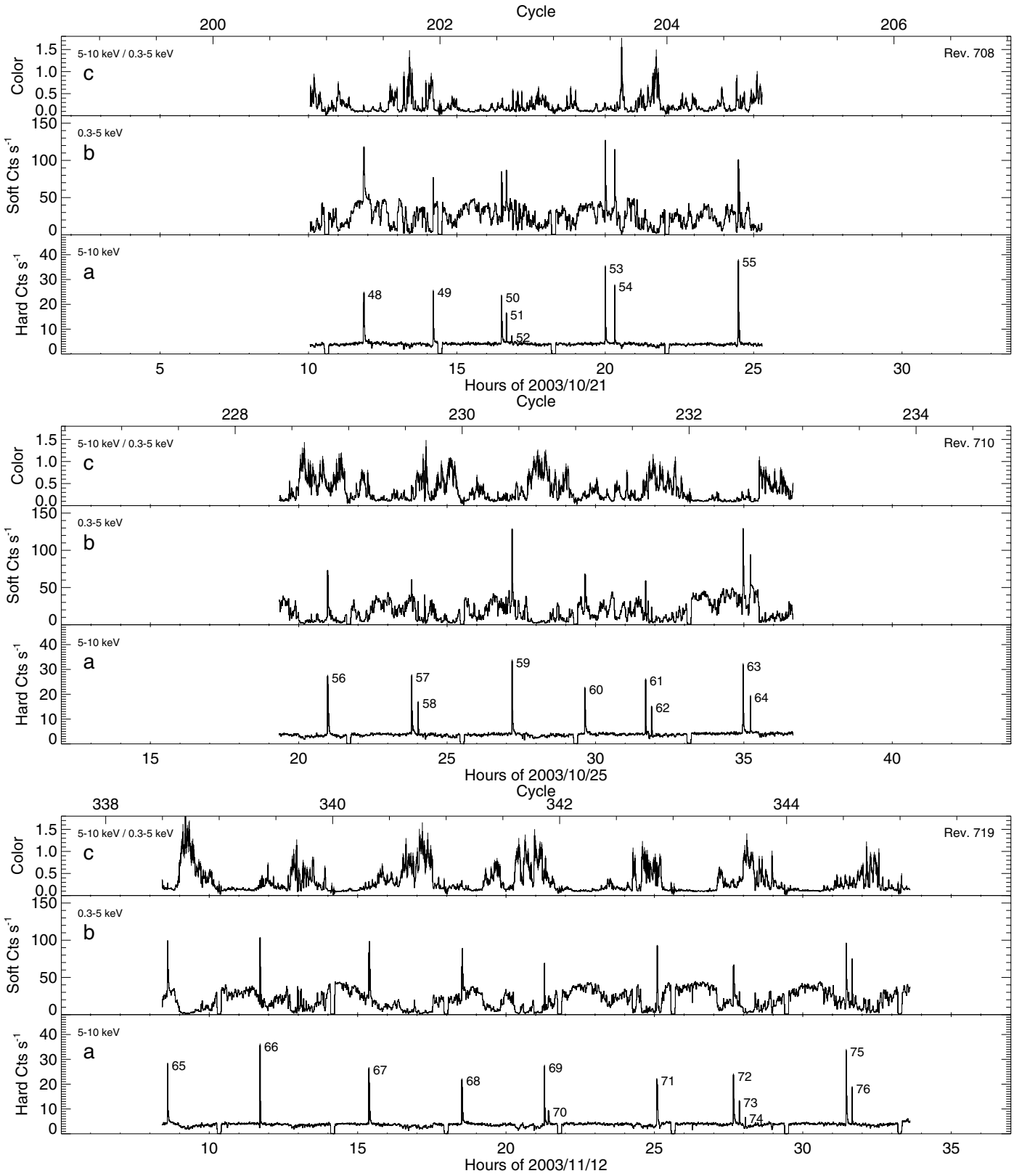

Fig. A.1. continued, for XMM-Newton revolutions 708 (*top*), 710 (*middle*) and 719 (*bottom*).

Table A.1. Bursts timing. The columns indicate the burst number, the XMM-Newton revolution number at which the burst occurred, the burst peak time determined from the EPIC PN 5–10 keV 1 s resolution light curve (except for burst 39 detected only by RGS), the wait time and the burst type. S means single burst. D1 and D2 mean first and second burst in a doublet. T1, T2 and T3 mean first, second and third burst in a triplet, respectively. When the burst type cannot be determined certainly, we indicate the different possible types, starting with the one attributed to the burst in this analysis.

Burst	Rev.	Peak time (UT)	$t_{\rm wait}$ (h)	Type	
1	692	Sep. 19 15:13:58	1.62<	S1	
2		19:52:12	4.64	S1	
3		23:04:31	3.21	S1	
4		20 01:36:43	2.54	D1	(T2)
5		01:46:28	0.162	D2	(T3)
6		05:21:42	3.59	S1	(D2)
7		07:58:35	2.61	D1	
8		08:10:17	0.195	D2	
9		11:31:58	3.36	S1	
10		13:57:49	2.43	S1	(D1, T1)
11	693	21 13:53:56	0.259< <23.9	S1	(D2, T3)
12		16:08:03	2.24	S1	
13		18:32:55	2.41	T1	
14		18:43:22	0.174	T2	
15		18:55:05	0.195	T3	
16		23:15:33	4.34	S1	(D2)
17		22 02:09:52	2.91	S1	
18		04:26:17	2.27	D1	
19		04:35:11	0.148	D2	
20		07:10:07	2.58	S1	(D2)
21		09:23:54	2.23	S1	
22		11:37:24	2.23	T1	
23		11:51:07	0.229	T2	
24		12:04:08	0.217	T3	
25	694	23 12:32:29	1.83< <24.5	S1	
26		15:05:56	2.56	S1	
27		17:25:09	2.32	S1	(D2)
28		20:00:08	2.58	S1	
29		22:34:36	2.57	D1	
30		22:45:51	0.187	D2	
31		24 02:10:45	3.41	D1	
32		02:26:15	0.259	D2	
33		06:03:06	3.61	S1	
34		08:50:34	2.79	T1	
35		09:05:55	0.256	T2	
36		09:16:31	0.177	T3	
37		13:36:43	4.34	S1	
38		16:37:55	3.02	S1	(D1, T1)
[a]39	695	25 17:28:20	0.036< <24.8	D1	(T2)
40		17:41:31	0.220	D2	(T3)
41		21:34:54	3.89	S1	
42		26 00:28:00	2.89	D1	
43		00:46:20	0.306	D2	
44		04:28:35	3.70	D1	
45		04:44:35	0.267	D2	
46		08:51:35	4.12	S1	
47		11:41:43	2.84	S1	
48	708	Oct. 21 11:51:35	1.82< <600	S1	(D1)
49		14:12:10	2.34	S1	(D1)
50		16:30:24	2.30	T1	
51		16:39:49	0.157	T2	
52		16:51:05	0.188	T3	
53		19:59:49	3.15	D1	
54		20:18:52	0.317	D2	
55		22 00:28:46	4.17	S1	
56	710	25 20:58:42	1.65< <92.5	S1	
57		23:48:23	2.83	D1	
58		26 00:01:37	0.221	D2	
59		03:11:08	3.16	S1	(D1)
60		05:38:40	2.46	S1	(D2)
61		07:41:16	2.04	D1	
62		07:53:28	0.203	D2	
63		10:58:02	3.08	D1	
64		11:13:05	0.251	D2	
65	719	Nov. 12 08:35:44	0.191< <405	S1	(D2, T3)
66		11:42:47	3.12	S1	
67		15:23:00	3.67	S1	
68		18:31:01	3.13	S1	
69		21:17:46	2.78	D1	
70		21:26:09	0.140	D2	
71		13 01:04:58	3.65	S1	
72		03:39:57	2.58	T1	
73		03:51:47	0.197	T2	
74		04:03:36	0.197	T3	
75		07:27:43	3.40	D1	
76		07:39:37	0.198	D2	

[a] detected by RGS only, before EPIC cameras were turned on.